

# Precipitation extremes in Ukraine from 1979 to 2019: Climatology, large-scale flow conditions, and moisture sources

Ellina Agayar<sup>1,2</sup>, Franziska Aemisegger<sup>1</sup>, Moshe Armon<sup>1</sup>, Alexander Scherrmann<sup>1</sup>, and Heini Wernli<sup>1</sup>

<sup>1</sup>Institute for Atmospheric and Climate Science, ETH Zürich, Zürich, Switzerland

<sup>2</sup>Odesa State Environmental University, Odesa, Ukraine

*Correspondence to:* Ellina Agayar (ellina.agayar@env.ethz.ch)

**Abstract.** Understanding extreme precipitation events (EPEs) and their underlying dynamical processes and moisture transport patterns is essential to mitigate EPE-related risks. In this study, we investigate the dynamics of 82 EPEs ( $\geq 100 \text{ mm}\cdot\text{day}^{-1}$ ) over the territory of Ukraine in the recent decades (1979-2019), of which the majority occurred in summer. The EPEs are identified based on precipitation observations from 215 meteorological stations and posts in Ukraine. The atmospheric variables for the case study analysis of selected EPEs and for climatological composites and trajectory calculations were taken from ERA5 reanalyses. Moisture sources contributing to the EPEs in Ukraine are identified with kinematic backward trajectories and the subsequent application of a moisture source identification scheme based on the humidity mass budget along these trajectories. The large-scale atmospheric circulation associated with EPEs was studied for a selection of representative EPEs in all seasons and with the aid of composites of all events per season. Results show that EPEs in summer occur all across Ukraine, but in other seasons EPE hotspots are mainly in the Carpathians and along the Black and Azov Seas. All EPEs were associated with a surface cyclone, and most with an upper-level trough, except for the winter events that occurred in situations with very strong westerly jets. Isentropic potential vorticity anomalies associated with EPEs in Ukraine show clear dipole structures in all seasons, however, interestingly with a different orientation of these anomaly dipoles between seasons. The analysis of moisture sources revealed a very strong case-to-case variability and often a combination of local and remote sources. Oceanic sources dominate in winter, but land evapotranspiration accounts for 60-80% of the moisture that rains out in EPEs in the other seasons. Taken together, these findings provide novel insight into large-scale characteristics of EPE in Ukraine, in a region with a unique geographical setting and with moisture sources as diverse as Newfoundland, the Azores, the Caspian Sea, and the Arctic Ocean.

**Keywords:** extreme precipitation events, Ukraine, potential vorticity anomalies, large-scale circulation, moisture sources

## 1 Introduction

Anthropogenic climate change not only affects mean climate conditions, but changes are also expected in the temporal variability of extreme meteorological events, including precipitation. Extreme precipitation events (EPEs) can lead to severe socioeconomic impacts and are expected to change in severity, frequency, and duration because of anthropogenic global warming (IPCC, 2021). EPEs pose a great threat as a trigger for landslides and floods (Jonkman, 2005; Barton et al., 2016; Jonkeren et al., 2014; Madsen et al., 2014; Moore et al., 2020). They are one of the most frequent natural hazards as documented for many regions of the world (Winschall et al., 2014; Santos et al., 2016; Li and Wang, 2018; Mastrantonas et al. 2020; Mastrantonas et al., 2021; Gao and Mathur, 2021; Giuntoli et al., 2021; Armon et al., 2023), and Ukraine is not an exception.

Ukraine is characterized by a quite complex orography. In the west and south-east are mountain ranges the Carpathians (Hoverla) and the Crimean Mountains (Roman-Kosh), with maximum elevations of 2061 m and 1545 m, respectively. In the south are the Black and Azov Seas, and most of the territory is characterized by hills (with typical heights of 200-300 m) and low-land plains. The extended geographical domain covered by the country includes a variety of climatic zones, e.g., the climate of the mountain tundra in the Carpathians and the Crimean Mountains, and subtropical climate along the southern coast of Crimea. Effects of continentality increase from west to east. Maritime air frequently passes over Ukraine from the North Atlantic, the Mediterranean, and the Arctic seas. In periods without advection of maritime air, continental conditions prevail with air circulating over the Eurasia plains (Lipinskyi et al., 2003). Recent studies already documented ongoing

50 climatic changes in Ukraine using observations and numerical model simulations (e.g., Semerhei-Chumachenko et al., 2020;  
51 Martazinova et al., 2018; Osadchy et al., 2012). These changes also lead to a dramatic increase in average annual economic  
52 losses due to flooding. An example is the flood in Transcarpathia in the period 21-27 June 2008, and a catastrophic flood in  
53 summer 2020, when in five regions in the west of the country, floods affected at least 250 settlements, damaged 750 km of  
54 roads, and 4 people died (Ukrainian State Agency of Water Resources, 2020; Mykhailiuk, 2022).

55 The genesis and spatiotemporal variability of EPEs in midlatitude regions are a consequence of complex dynamical and  
56 thermodynamical processes that occur on the synoptic and mesoscale. The nature of these processes is determined both by  
57 the large-scale atmospheric flow, leading to a strong increase in moisture transport to the EPE region, and the influence of  
58 deep convective systems. For instance, short-term EPEs usually are a consequence of intense convection. In contrast, EPEs  
59 accumulated over 1–3 days are often associated with the passage of an atmospheric front (Catto and Pfahl, 2013), with  
60 upper-level Rossby wave breaking (Massacand et al., 1998; Moore et al., 2019; de Vries, 2021), and also cyclones and  
61 blocking systems were shown to be especially relevant for EPEs (Pfahl 2014; Priestley et al., 2017; Agel et al., 2018;  
62 Tuel et al., 2022). It is quite common for heavy precipitation to occur in synoptic configurations at the interface between  
63 high-pressure disturbances and cyclones (Breugem et al., 2020). According to Pfahl and Wernli (2012), in many regions,  
64 cyclones are linked with a large percentage of EPEs. Cyclones and anticyclones both play an important role in moisture  
65 transport, while cyclones typically also go along with forcing for ascent, in combination leading to EPEs. Blocking  
66 anticyclones in addition effectively hinder the usual westerly large-scale atmospheric flow, resulting in persistent flow  
67 anomalies in and around the blocked region. Their presence and characteristics significantly impact the predictability of  
68 weather extremes (Rex, 1950a; Lenggenhager et al., 2019; Kautz et al., 2022), including EPEs. Furthermore, extreme  
69 precipitation is often associated with atmospheric blocking and coexisting upper-tropospheric cutoffs (Portmann et al., 2021).  
70 A key aspect of EPEs that gained increased attention in the last years, is the analysis of moisture sources. For instance, James  
71 and Stohl (2004) and Sodemann et al. (2008) developed trajectory-based methods to objectively identify evaporative regions  
72 that later contribute to intense rainfall in the region of the EPE. Such methods have been applied to identify the moisture  
73 sources globally (Gimeno et al., 2012; Sodemann, 2020; for selected EPEs in Europe (e.g., Grams et al. 2014; Raveh-Rubin  
74 and Wernli, 2017) for climatological analyses of precipitation in the Alpine region (Sodemann and Zubler 2009), the  
75 Mediterranean (Ciric et al., 2018), the USA (e.g., Yang et al., 2023) in South Asia (Bohlinger et al., 2017), and in the  
76 Arabian Peninsula (Horan et al., 2023). However there has not been much research on the hydrological cycle in Ukraine  
77 since the study by Budyko and Drozdov (1953), and moisture sources for EPEs in this domain have not been investigated yet.  
78 In this study, we consider precipitation observations to identify EPEs for the territory of Ukraine in the last 40 years and  
79 study their characteristics in terms of the large-scale flow and moisture source conditions. For this, we use the ERA5 dataset,  
80 which is the fifth-generation reanalysis from the European Centre for Medium-range Weather Forecasts (ECMWF) that is  
81 available since 1940 (Hersbach et al., 2020). ERA5 provides hourly estimates for a large number of atmospheric, ocean-  
82 wave and land-surface quantities. The novelty is in the application of a systematic climatological approach to study the large-  
83 scale characteristics of EPEs in Ukraine and their moisture sources. Given the geographical setting of Ukraine, with its  
84 proximity to the Black Sea, the eastern Mediterranean, but also the Baltic and the Caspian Seas, the most important moisture  
85 sources are not obvious and require careful analysis. Using the ERA5 dataset, anomalous characteristics of the flow situation  
86 associated with EPEs can be identified, including potential vorticity (PV) and wind speed at different levels, in all seasons.  
87 More specifically, this study is guided by the following key questions:

- 88 • 1: What is the seasonality of EPEs in Ukraine, and how are EPEs distributed spatially and temporally?
- 89 • 2: What are the distinctive tropospheric flow conditions during EPEs?
- 90 • 3: What are the geographical moisture sources of EPEs in Ukraine in the different seasons?

91 • 4: What is the distinction between individual cases with diverse large-scale flow conditions and moisture source origins?  
92 The paper is organized as follows. In Sect. 2 we introduce the datasets and methods. Then, in Sect. 3, a climatological  
93 overview of EPEs is presented (Sect. 3.1). In Sect. 3.2, we discuss anomalies of pressure and summer moisture anomalies of  
94 EPEs, in Sect. 3.3 we analyze PV and wind anomalies associated with EPEs. Seasonal moisture source identification  
95 (Sect. 3.4) and selected case studies of EPEs illustrate the main large-scale processes involved (Sect. 3.5). A summary and  
96 conclusions are given in Sect. 4.

97

## 98 **2 Data and methodology**

99

### 100 **2.1 Identification of EPEs**

101

102 For this study, 215 meteorological stations and posts (including aviation weather stations, gauging stations, etc.) with daily  
103 data from 1979 to 2019 are used. From this dataset, 183 stations were selected for our study that have a complete set of data.  
104 The remaining 32 stations did not have the same record length for various reasons. Nevertheless, these stations were still  
105 tested for the occurrence of EPEs, but no extreme events were found according to our criteria (see below). Due to the  
106 absence of data in the Ukrainian meteorological network for certain regions of Crimea from February 2015 to December  
107 2019, additional data were obtained using open-access observations for this region (SYNOP observational data).  
108 Unfortunately, data for four stations in the Donetsk and Lugansk regions for the period of 2015-2019 are not openly  
109 available. In this region, a 36-year dataset was employed to identify days with extreme precipitation.

110 Our criterion to identify EPEs was a threshold of  $100 \text{ mm}\cdot\text{day}^{-1}$ . With this criterion, in total 82 EPEs were identified.  
111 Table S1 in the Supplement lists the date and station for each of these events. Our threshold of  $100 \text{ mm}\cdot\text{day}^{-1}$ , is chosen from  
112 expert knowledge, as it is often used to define EPEs in different countries. For instance, Martin-Vide et al. (2008) used this  
113 threshold to determine EPEs in the western Mediterranean, and Trambly et al. (2013) in southern France. Boissier and Vinet  
114 (2009) identified the value of  $100 \text{ mm}\cdot\text{day}^{-1}$  as a critical threshold that could trigger fatalities. Also in Ukraine, this threshold  
115 is used to identify an event as extreme. Given that we considered a 40 year time period and that EPEs were identified at each  
116 station between 0 and 3 times (see Table S1), we can estimate that our threshold corresponds to the 99.8th percentile or  
117 higher. These percentiles highlight that the selected threshold of  $\geq 100 \text{ mm}\cdot\text{day}^{-1}$  indeed selects extreme, i.e., very rare events.  
118 These events are so rare that we cannot robustly assess regional differences of percentiles. The largest amount of recorded  
119 precipitation occurred with  $278 \text{ mm}\cdot\text{day}^{-1}$  on 2 Sep 1981 in Karadag (in the southeast of Crimea). Another exceptional event  
120 occurred in Ai-Petry (in the south of Crimea) with 228 mm on 27 and 28 Dec 1999 (accumulated over two days). An  
121 overview of the seasonal and geographical distribution of the EPEs will be given in Sect. 3.1.

122

### 123 **2.2 Dynamical Characterization**

124

125 For the dynamical investigation of the EPEs, selected fields from ERA5 reanalyses from the ECMWF were used. All  
126 reanalysis data were interpolated to a  $0.5^\circ$  grid. Specifically, we analyzed the following variables, characterizing the large-  
127 scale flow: mean sea level pressure (MSLP), wind speed at 300 hPa, geopotential height at 500 hPa, PV on different  
128 isentropic surfaces, total precipitation, total column water (TCW) and convective available potential energy (CAPE).  
129 Composites were calculated as the mean of all values during EPE days and anomalies were computed as deviations between  
130 the seasonal average and the mean EPE conditions. To overcome biases related to intra-season differences in the number of  
131 identified EPEs (e.g., no events occur in January and April), we corrected the above-mentioned composite anomalies with

132 this frequency bias of EPEs serving as a weight for the seasonal averaging. Consideration of such standardized anomalies for  
133 EPE events can help recognize typical flow conditions and potential precursors for EPEs in Ukraine.

134

## 135 **2.3 Moisture Sources**

136

137 We used the Lagrangian Analysis Tool LAGRANTO (Sprenger and Wernli, 2015) and 3-dimensional wind fields from  
138 ERA5 to compute 10-day backward trajectories from the regions affected by EPEs. For the identification of moisture sources,  
139 we used the method introduced by Sodemann et al. (2008), which relies on the evolution of specific humidity along the  
140 trajectories. An analogous trajectory-based approach has been used previously for identifying moisture sources of  
141 precipitation in, e.g., intense North Atlantic cyclones (Aemisegger, 2018; Papritz et al., 2021), Mediterranean cyclones  
142 (Krug et al., 2022), and for a climatological analysis of the global water cycle (Sodemann, 2020). We started the trajectories  
143 every hour on the day of the EPE and every 20 hPa between 1000 and 200 hPa from the location of the station, where the  
144 EPE occurred. Trajectories were considered for the moisture source diagnostic if their relative humidity at the arrival point  
145 exceeded 80%. Since the global mean atmospheric moisture residence time is about 4–5 days (Läderach and Sodemann,  
146 2016) the 10-day backward trajectories cover a large part of the moisture sources of the total precipitation, with explained  
147 fractions of 85 to 97%. Moisture source regions were identified by diagnosing hourly changes in specific humidity along the  
148 air parcel trajectories, and assuming that increases in specific humidity result from surface evaporation and decreases from  
149 precipitation. Evaporation is identified where the hourly increase of specific humidity exceeds  $0.025 \text{ g}\cdot\text{kg}^{-1}\cdot\text{h}^{-1}$ . These  
150 moisture uptakes were taken into account both in and above the boundary layer, since convective injections of vapour from  
151 the boundary layer can also occur in the free troposphere (Aemisegger et al., 2014). When precipitation occurs (identified as  
152 decreases in specific humidity), the contribution of the previous uptakes are discounted proportionally to their share in the  
153 humidity loss (Sodemann et al., 2008). This moisture source diagnostic was applied to the hourly trajectories for all EPE  
154 days, and moisture uptake maps were calculated for each EPE. For the climatological analysis four seasonal composite maps  
155 were calculated by weighting each event by its total measured precipitation.

156

## 157 **3 Results**

158

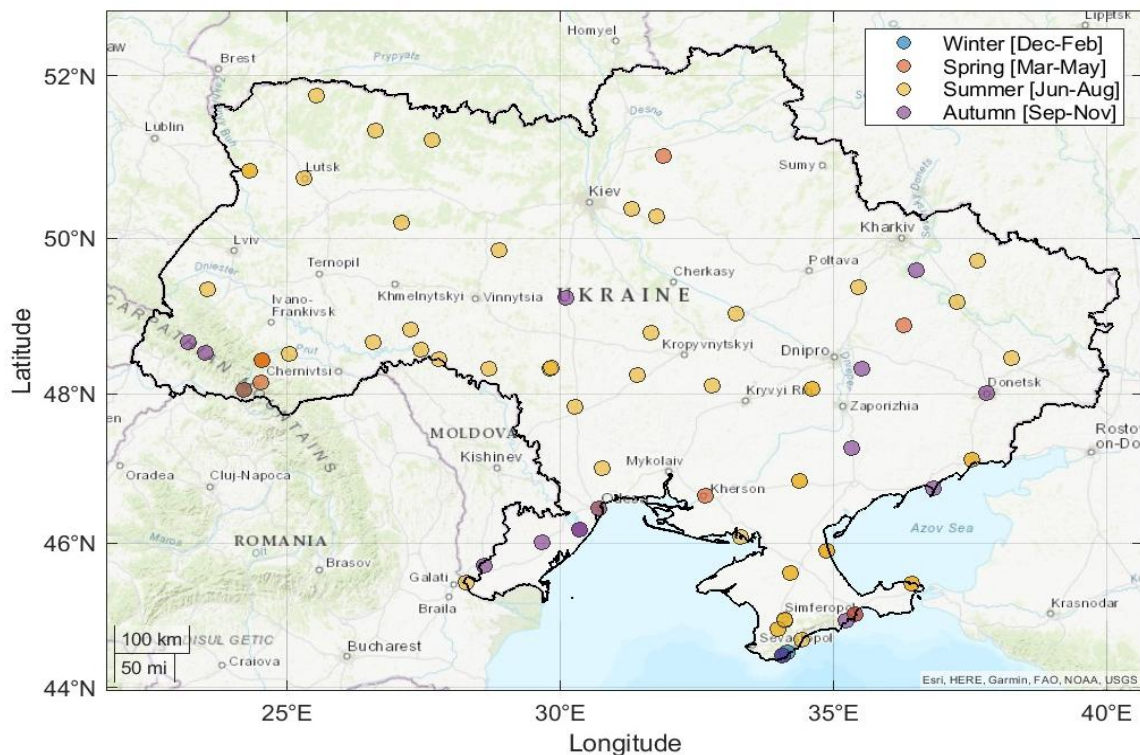
### 159 **3.1 Spatiotemporal distribution of EPEs over Ukraine**

160

161 Precipitation in Ukraine generally exhibits a diminishing trend from the north and northwest to the south and southeast areas  
162 (Lipinskyi et al., 2011). In the mountainous areas, orographic lifting contributes to enhanced precipitation. As a result, the  
163 Ukrainian Carpathians and the Crimean Mountains experience the largest precipitation values (annual total >1000 mm). In  
164 the central and eastern parts of Ukraine, the amount of annual precipitation is 550 - 650 mm; the southern part, along the  
165 coast of the Black Sea, is comparatively dry (annual total 380 – 400 mm). In the cold season, approximately 20–25% of the  
166 annual precipitation occurs, contrasting with the warm period, where 75–80% of the total annual precipitation is recorded.  
167 During the warmer season, the precipitation distribution reflects the annual pattern, with a gradual decrease from the  
168 northwest to the southeast, reaching 300 mm or less in the coastal regions.

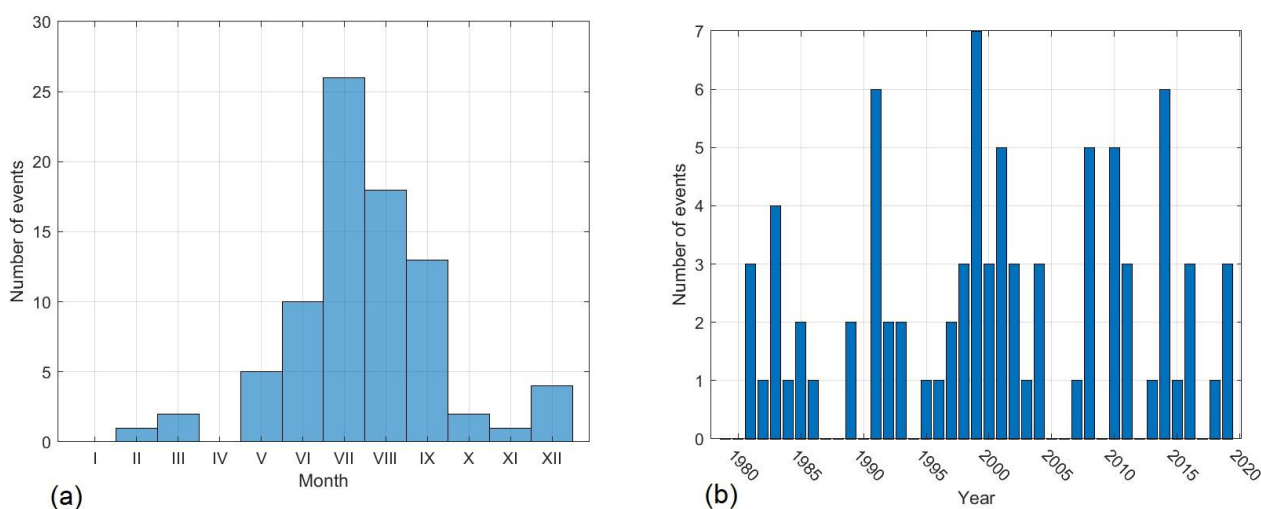
169 In the study period, the 82 EPEs identified with a threshold of  $100 \text{ mm day}^{-1}$ , were observed at stations in almost all regions  
170 of Ukraine, except Sumy, Luhansk and Cherkasy (Fig. 1). Their distribution has a clear seasonality. The highest number of  
171 EPEs occurred in summer (June, July, August) with 54 cases, with a peak in July with 27 cases (Fig. 2a). In the Northern  
172 Black Sea region and on the Crimean Peninsula, 18 summer events were observed, two of them with more than

173 130 mm·day<sup>-1</sup>. For example, in the Odesa region at Serbka station, 148.4 mm·day<sup>-1</sup> were recorded on 27 June 1996, and at  
 174 the station Pochtove in Crimea, 137.8 mm·day<sup>-1</sup> on 23 July 2002. Several summer EPEs were also noted in the central,  
 175 western, and eastern regions of Ukraine. The most intense precipitation in these areas was recorded at the Loshkarevka  
 176 station in the Dnepropetrovsk region with 154.2 mm·day<sup>-1</sup> on 5 July 1983 and at the Barishevka station in the Kyiv region  
 177



178  
 179  
 180  
 181  
 182  
 183

**Figure 1** The identified 82 EPEs at stations in Ukraine in the period 1979-2019. Colors show the season of occurrence. Please note some of the stations recorded more than one EPE. Ukraine shapefile source: <https://gadm.org/maps/UKR.html>



184  
 185  
 186  
 187

**Figure 2** (a) Seasonal cycle (sum of monthly occurrence values) and (b) time series of annual number of EPEs in Ukraine in 1979-2019.

188 with  $130.7 \text{ mm}\cdot\text{day}^{-1}$  on 1 July 2011. In autumn, 16 cases of extreme precipitation were recorded, mainly in the west and  
189 south of Ukraine (meteorological stations located in the Transcarpathia and Odesa regions, as well as in Crimea). All autumn  
190 EPEs occurred in September, except for three cases (12 Oct 2016 - Bolgrad, 29 Oct 1992 - Play, and 4 Nov 1998 -  
191 Mizhirgya). One EPE was noted on the territory of the Crimean Peninsula at Karadag on 1 Sep 1991 with  $278 \text{ mm}\cdot\text{day}^{-1}$ .  
192 This particularly high value most likely reveals a strong orographic effect on the intensity of EPEs in this region. At  
193 Belgorod-Dnestrovsky station (the Black Sea coast), two EPEs were recorded during the study period, both in September, on  
194 21 Sep 2008 ( $100.2 \text{ mm}\cdot\text{day}^{-1}$ ) and on 20 Sep 2016 ( $135.2 \text{ mm}\cdot\text{day}^{-1}$ ). In spring, seven EPEs were identified in Ukraine,  
195 mainly in the Ivano-Frankivsk and Zakarpattia regions, as well as in the Crimea. The intensity of precipitation in spring did  
196 not exceed  $116.9 \text{ mm}\cdot\text{day}^{-1}$  (on 5 March 2001, station Pozhezhevskaya). The lowest occurrence of EPEs was in the winter,  
197 with only five events that all occurred in the south of Crimea, four of them in December and one in February. At the  
198 mountain station Ai-Petri  $112.5$  and  $115.3 \text{ mm}\cdot\text{day}^{-1}$  were observed on 27-28 Dec 1999, and at Yalta  $100 \text{ mm}\cdot\text{day}^{-1}$  were  
199 measured on 28 Dec 1999.

200 The number of EPEs in Ukraine varies from year to year. Actually, they were registered annually, with the exception of a  
201 few years (Fig. 2b). In 1991, 1999, and 2014 the number of EPEs rose to 6-7 cases. However, there is no obvious trend in the  
202 frequency of EPEs that are identified with the threshold of  $100 \text{ mm}\cdot\text{day}^{-1}$ .

### 203 204 **3.2 Dynamical characterization: seasonal-mean flow composites**

205  
206 In this section, we analyze the dynamic conditions for the occurrence of EPEs in Ukraine, separately for each season. Figure  
207 3 presents the composites of the anomalies of MSLP, geopotential height and the horizontal wind at 500 hPa on EPE days.  
208 We first discuss these flow anomalies for all four seasons, and then, put a focus on summer, when most EPEs occurred,  
209 where we consider anomalies of total precipitation, CAPE and TCW in Fig. 4. (For completeness, the anomaly maps of these  
210 fields for the other seasons can be found in the supplementary Fig. S1).

211 On winter EPE days (Fig. 3a), there is a strong negative geopotential height anomaly over Eastern Europe, with a peak value  
212 of 241 m. This upper-level trough located above a baroclinic zone causes the formation of a cyclone in the lower troposphere.  
213 The center of the negative MSLP anomaly is located over the Carpathian region (Hungary and Romania) and reaches values  
214 up to 24 hPa below average. A second local MSLP anomaly is found over eastern Ukraine ( $-20$  hPa). The strong cyclones  
215 over southwest Europe on EPE days go along with a strongly intensified jet stream over the northern Mediterranean, Turkey,  
216 and the Black Sea (maximum 500 hPa wind speed anomalies up to  $20 \text{ m}\cdot\text{s}^{-1}$ ). The intense low-pressure systems developing  
217 over west and southwest Ukraine led to EPEs in the southwestern Ukraine, particularly in Transcarpathia region and on the  
218 coast of Crimea, where frontal precipitation is reinforced by orographic uplift on the windward sides of mountain ranges.

219 In all other seasons, 500-hPa geopotential height anomalies on EPE days are much weaker than in winter, but negative  
220 anomalies extend over Ukraine in all seasons. In spring (Fig. 3b), the negative anomaly reaches a maximum amplitude of  
221  $-48$  m. The low-pressure zone covers the entire territory of Ukraine (MSLP anomaly of  $-6$  hPa) and weak 500-hPa wind  
222 anomalies curve cyclonically over the Balkans toward the Black Sea. These synoptic conditions led to the emergence of  
223 EPEs mainly in the southern regions of Ukraine and Crimea. In autumn (Fig. 3d), a negative 500-hPa geopotential height  
224 anomaly is identified over the entire territory of Ukraine, which is strongest in the southeast with peak values of  $-79$  m. At  
225 the same time, there is a strong negative MSLP anomaly (up to  $-12$  hPa) with its core located over eastern Ukraine. The  
226 wind anomaly in the middle troposphere shows again a cyclonic flow, in agreement with the negative geopotential height  
227 anomaly.

228

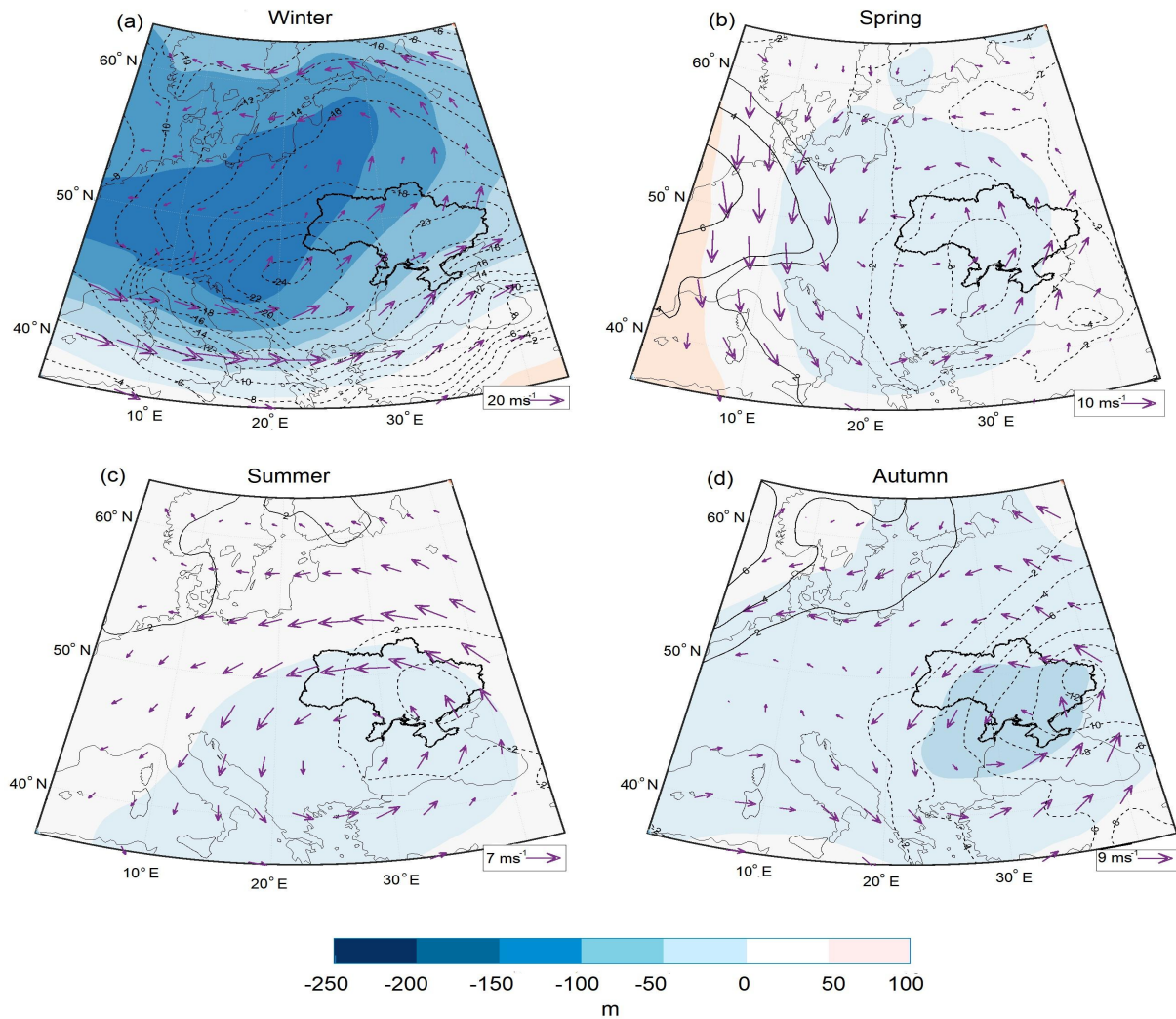
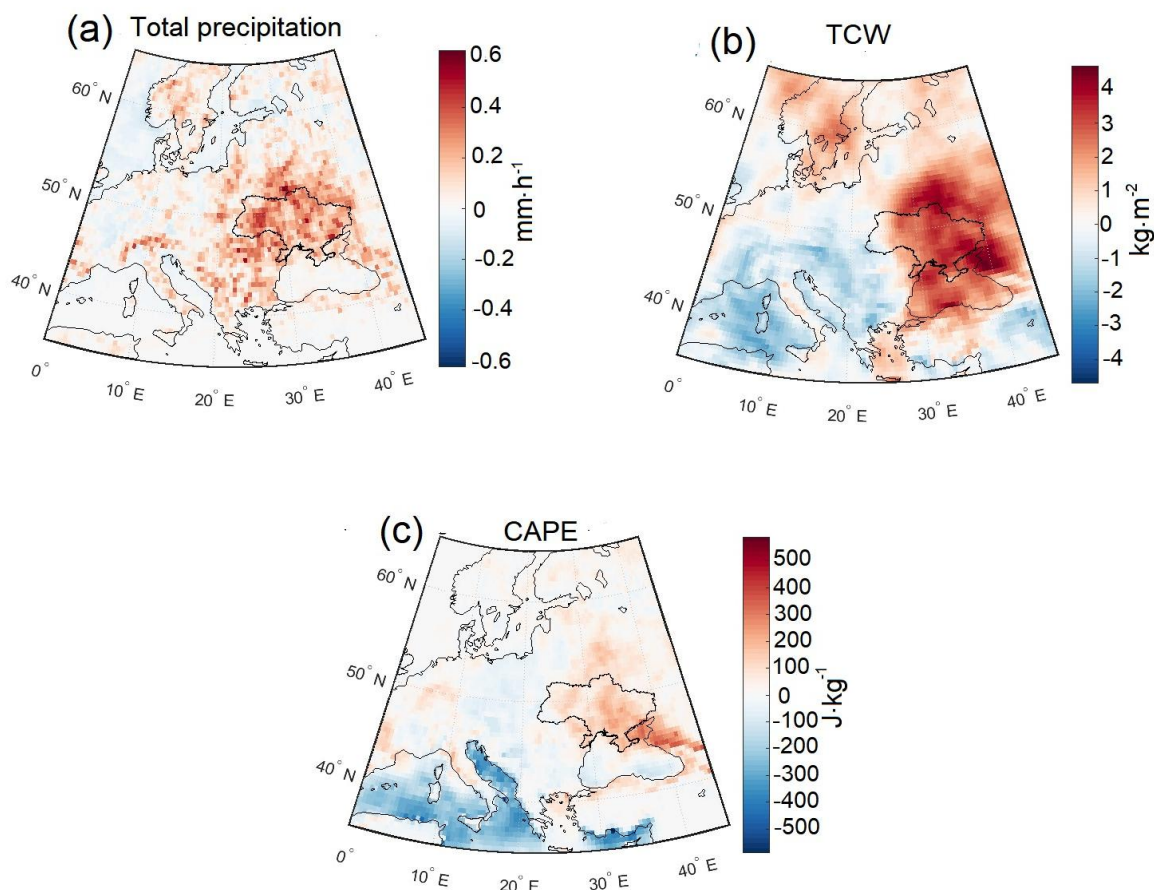


**Figure 3** Seasonal composites on EPE days of anomalies of geopotential height at 500 hPa (colors, in m), MLSP (in hPa, solid and dashed contours for positive and negative values, respectively), and 500-hPa winds (purple arrows, reference vector is shown in lower right corner, in  $\text{m}\cdot\text{s}^{-1}$ ).

Last but not least, in summer, when most EPEs occurred, surface pressure and 500-hPa level anomalies revealed a weak-gradient depression with a low-pressure center shifted to the southeast of Ukraine ( $-4$  hPa). The negative 500-hPa level anomaly stretched from the central Mediterranean through the Balkans, reaching peak values of  $-43$  m. Wind anomalies at the 500-hPa level over Ukraine were primarily from the east; however, they were weaker compared to those in other seasons and did not exceed  $8$   $\text{m}\cdot\text{s}^{-1}$  (Fig. 3c). EPEs were observed throughout the domain under these large-scale flow structures, but were due to different reasons. EPE in the central and southeast parts coincided with the low anomaly center, indicating that their main cause was dynamical lifting. However, small-scale processes associated with strong convection also played a significant role, as well as orographic ascent along the windward slopes of the Crimean and Carpathian Mountains. The thermodynamic composites shown in Fig. 4 for the summer EPEs provide valuable additional information. Figure 4a reveals that days with an EPE occurring at one station had on average anomalously high precipitation in the entire territory of Ukraine and beyond. Precipitation anomalies exceed  $0.6$   $\text{mm}\cdot\text{h}^{-1}$  along a band from north to south, stretching through the Podolsk Upland to the Black Sea. Other local maxima were observed in the southeast, including the Donetsk Ridge, the

247 Azov Sea, and Crimea. Positive total column water anomalies (up to more than 4 kg m<sup>-2</sup>) extend over all of Ukraine, except  
248 the Transcarpathian region (Fig. 4b).  
249



250

251

252 **Figure 4 Anomalies of total precipitation, TCW and CAPE at 15 UTC on EPE days in summer.**

253

254 This also contributes to increased CAPE (Fig. 4c), providing the necessary ingredients for convection (Rasmussen and  
255 Houze 2016). Thus, in summer, on days when EPEs occurred, elevated moisture levels progressed over the entire Ukraine,  
256 making the entire domain on average more humid than compared to normal conditions. The EPEs in Ukraine were triggered  
257 both by the large-scale ascent due to the upper-level cyclonic flow anomaly and the development of convection in the  
258 southeastern and eastern regions, as well as by local (orographic) convection in the central and western parts.

259 In summary, the primary reasons for the occurrence of extreme precipitation in all seasons were the presence of cyclonic  
260 anomalies generating anomalously moist flows and the triggering of convection in the affected regions. In summer, the  
261 greatest contribution to the formation of EPEs was from convective processes, both frontal and local. Total column water  
262 values were, on average, increased, mainly over the eastern regions in winter and autumn, and over the entire Ukraine in  
263 spring and summer (Figs. 4b and S1). This suggests that moisture characteristics are essential for understanding the process  
264 of extreme precipitation formation. Therefore Sect. 3.4 is dedicated to defining the origin, uptake characteristics, and  
265 transport pathways of moisture that precipitates during EPEs in Ukraine. It is also worth highlighting the influence of  
266 orography on the formation of EPEs. Whereas over the flat terrain of Ukraine, dynamic uplift near the cyclone center is most  
267 important for the generation of extreme precipitation, in the mountainous regions of Ukraine, such as the Carpathians and  
268 Crimea, orographic enhancement of precipitation is crucial in the formation of the EPEs.

269

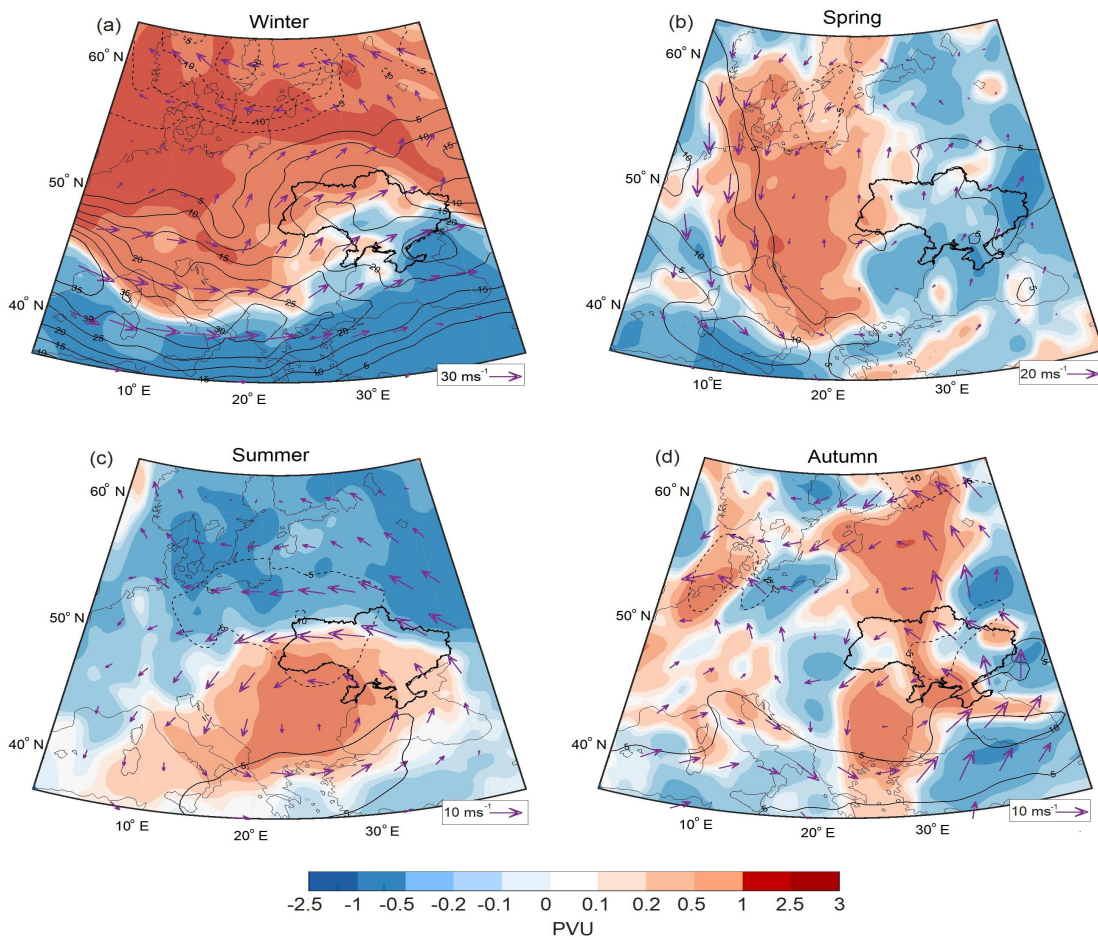


270 **3.3 Climatological characteristics of PV anomalies**

271

272 In all seasons the vertical coherence of the negative anomalies of geopotential height at 500 hPa and MSLP, which indicates  
 273 that EPEs typically co-occur with vertically deep extratropical cyclones that are associated with upper-level troughs or  
 274 cutoffs. This aspect can be further investigated by also considering the isentropic PV distribution on EPE days. Positive PV  
 275 anomalies on tropopause-intersecting isentropes are often linked with developing surface cyclones and severe weather  
 276 phenomena (Portmann et al., 2021), a different isentropic surface is most suitable to study upper-level PV dynamics in a  
 277 specific region during the different seasons. In this study, it turned out to be useful to select the following isentropes: 315 K  
 278 in winter, 325 K in spring, 335 K in summer, and 330 K in autumn. Figure 5 presents the composites of PV anomalies on  
 279 these isentropes and the 300-hPa wind (Fig. 5).

280



281

282

283 **Figure 5 Seasonal composites on EPE days of anomalies of isentropic PV (colors, in PVU), and of 300-hPa wind**  
 284 **(purple arrows, see reference vector in lower right corner, in  $m \cdot s^{-1}$ ) and wind speed (solid and dashed**  
 285 **contours for positive and negative values, respectively).**

286

287 On winter EPE days (Fig. 5a), there is a large positive PV anomaly extending over Europe (consistent with the negative  
 288 Z500 anomaly in Fig. 3a) with maximum values that exceed 2.5 PVU near 55°N stretching from the North Sea to southern  
 289 Russia. The flow induced by this PV anomaly leads to strong low-tropospheric winds toward the Crimean and Carpathian  
 290 Mountains causing orographic uplift (not shown). In the south of the depicted region, i.e., over most of the Mediterranean  
 291 and the Black Sea, there are large negative PV anomalies, and as a consequence, over Ukraine, PV anomalies are close to  
 292 zero but there is a strong poleward gradient of PV anomalies, which goes along with strongly increased westerly winds at the

293 300-hPa jet level (wind speed anomalies reached  $\sim 25\text{-}35\text{ m}\cdot\text{s}^{-1}$ ). Noteworthy is the strongly positive upper-level wind speed  
294 anomaly over the Crimea Peninsula and the Azov Sea, i.e., in the region where the most intense winter EPEs have been  
295 recorded.

296 In spring (Fig. 5b), the positive PV anomaly is more confined and extends meridionally from southern Scandinavia to the  
297 Adriatic Sea, with maximum values over the eastern Alps ( $+0.1\text{-}1\text{ PVU}$ ). This positive anomaly also reaches western Ukraine,  
298 but over the main territory of Ukraine, PV anomalies are weakly negative and increase in amplitude towards the east. A  
299 strong positive wind speed anomaly occurs along the western flank of the PV anomaly, and over Ukraine there is a weakly  
300 enhanced southerly flow at 300 hPa. Similarly to winter, the EPE regions were located east of the positive upper-level PV  
301 anomaly, in a region with an enhanced horizontal PV gradient and therefore upper-level flow.

302 In summer (Fig. 5c), the moderately intense positive PV anomaly is located over southeastern Europe, extending over most  
303 parts of Ukraine. In this season, negative PV anomalies occur at high latitudes, leading to a strongly different PV anomaly  
304 pattern compared to the other seasons. The summer PV anomaly over Eastern Europe reflects the occurrence of PV cutoffs,  
305 which repeatedly formed, locally changing the static stability, and thus providing the ideal mesoscale environment for the  
306 triggering of convection and EPEs, and the formation of cyclones over Ukraine. Also note, that the Black Sea region is  
307 characterized by a local maximum in the frequency of PV cutoffs in all seasons (Portmann et al., 2021). The wind speed  
308 anomaly at 300 hPa shows a well-defined cyclonic circulation with a pronounced easterly flow anomaly over Ukraine, in  
309 agreement with the equatorward gradient of the PV anomaly in this region.

310 Last, for EPEs in autumn (Fig. 5d), the positive PV anomaly is strongly meridionally oriented similarly to spring, but now  
311 extends directly over Ukraine. Negative PV anomalies are found over southern Poland and Slovakia, creating an eastward  
312 gradient of PV anomalies over western Ukraine and an anomalous northerly flow, leading to the emergence of orographically  
313 enhanced EPEs in Transcarpathia. Over the Black Sea and Eastern Ukraine, there is an enhanced southerly flow and the  
314 pronounced positive PV anomaly most likely contributed to the intensification of cyclones over eastern Ukraine (see Fig. 3d).  
315 The standardized anomaly pattern exhibits a seasonal variation, reaching its peak (approximately 1.7 SD) during winter and  
316 reaching a minimum of 0.7 SD in summer, in the main PV anomaly regions (supplementary Fig. S2). We note, however, that  
317 these fields should be regarded with caution in all seasons except summer, because of the low number of events.

318 In summary, during all seasons EPEs in Ukraine are associated with pronounced upper-level PV anomalies. As a common  
319 feature, in all seasons, the region of Ukraine is located between positive and negative PV anomalies. However, interestingly,  
320 the orientation of these anomaly dipoles differs strongly between the seasons, and can be classified, to first order, as  
321 northward in winter, westward in spring, southward in summer, and eastward in autumn. Consistent with the basic  
322 understanding of PV dynamics, these differently orientated PV anomaly dipoles lead to characteristics seasonal patterns of  
323 the anomalous upper-level flow, and also can influence the moisture transport process in the middle troposphere. In each  
324 season, EPEs appear to be preconditioned largely by a moist flow from the southwest, south, or southeast, along the eastern  
325 flank of the upper-level PV anomalies.

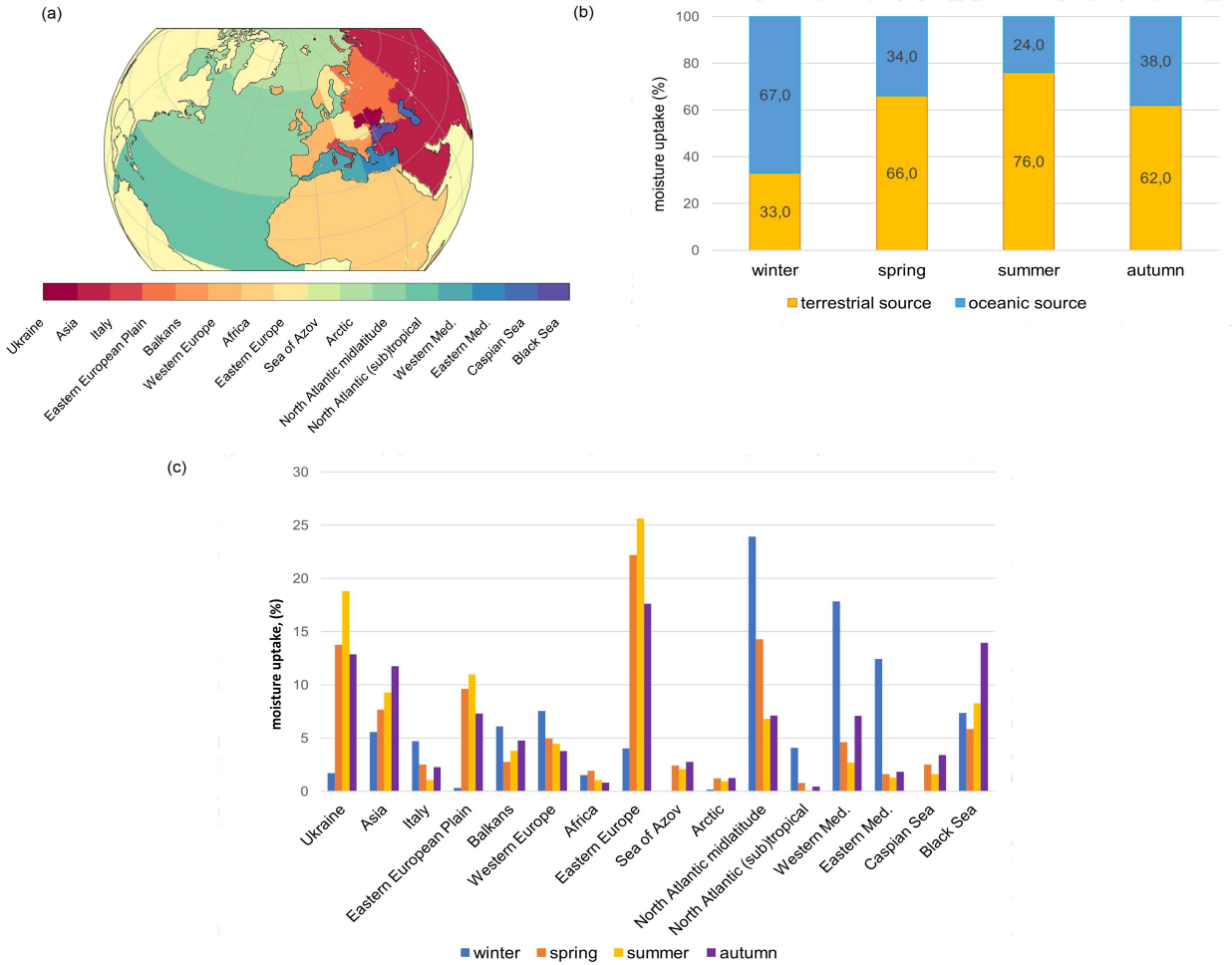
326

### 327 **3.4 Seasonal mean moisture sources**

328

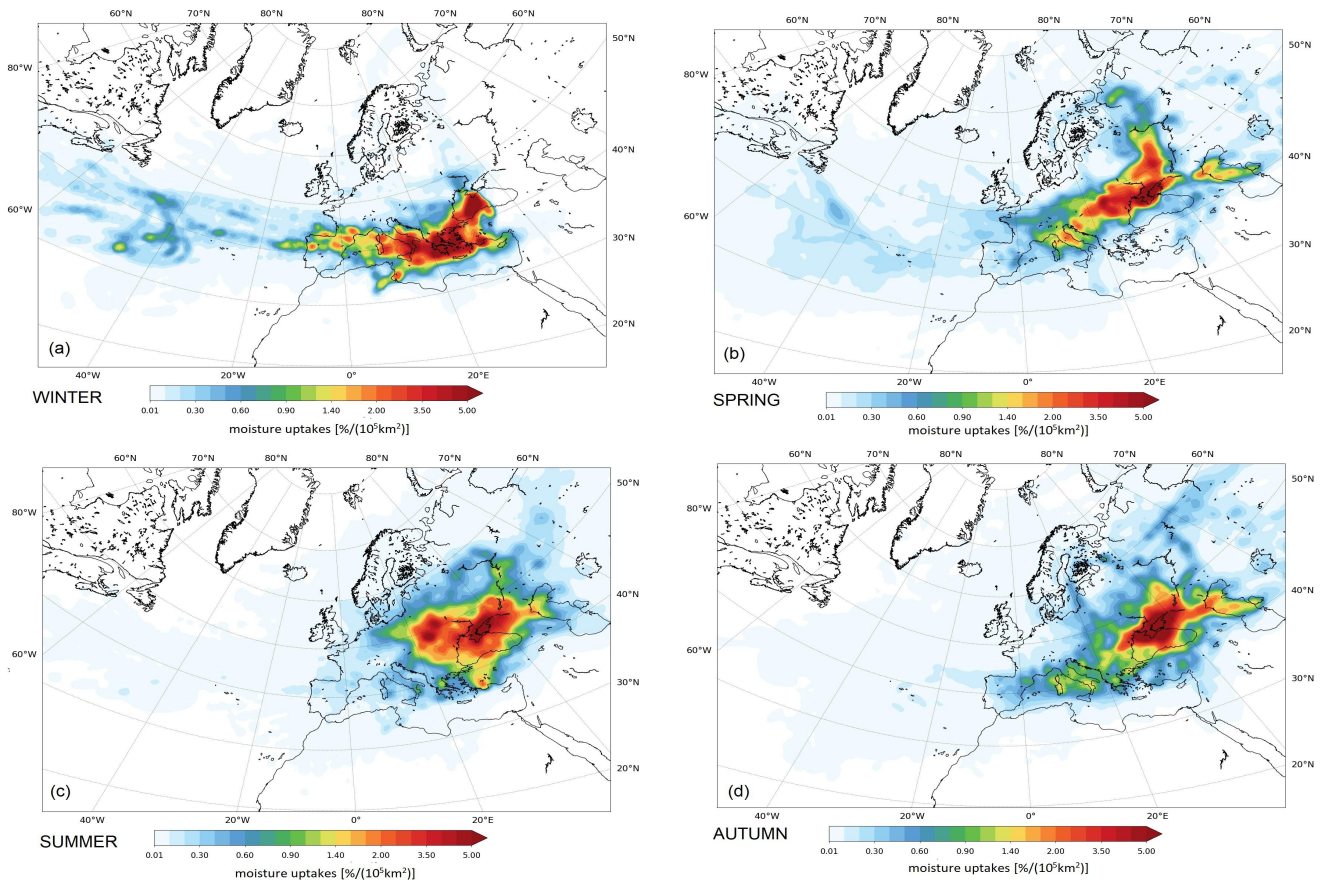
329 To categorize and summarize the various moisture source contributions of EPEs in Ukraine, we define large-scale source  
330 regions, separately for oceanic and terrestrial sources. As oceanic moisture sources, we include the midlatitude North  
331 Atlantic, the Mediterranean Sea (western and eastern parts, separately), the Black and Azov Seas, and the Caspian Sea.  
332 Terrestrial regions considered are western and eastern Europe, Italy and the Balkans, Ukraine, the East European Plain,  
333 Africa, and Asia (Fig. 6a). Figures 6b and 6c provide information about the percentage contribution from different moisture

334 sources for EPE in all seasons, and seasonal moisture uptake composites are shown in Fig. 7.  
 335 In winter, EPEs in Ukraine have predominantly oceanic moisture origins (67%, Fig. 6b). An elongated uptake zone is located  
 336 over the midlatitude North Atlantic (24%), in the western (18%) and eastern Mediterranean (12%), and the Black Sea (7%),  
 337 consistently with the strongly enhanced westerly flow discussed in Sect. 3.2. The share of terrestrial sources (34%) is smaller  
 338 than the oceanic contributions. The main land sources are western Europe (8%), the Balkans (6%), and Asia (6%). The  
 339 maximum moisture sources are located over the North Atlantic, the Mediterranean and the Black Sea.  
 340



341  
 342  
 343 **Figure 6 (a) Predefined moisture source regions; (c) shows their seasonal-mean relative contributions on EPE days**  
 344 **in Ukraine, and (b) shows these contributions aggregated to terrestrial and oceanic sources.**  
 345  
 346 In the other seasons, the moisture sources are predominantly over land (Fig. 6b). In spring, the total moisture contribution  
 347 from land surfaces increased to 66% (Fig. 6b), with local contributions of 22% from eastern Europe, and 14% of continental  
 348 recycling over Ukraine. The maximum moisture source is located over southern Ukraine and the Azov Sea (Fig. 7). A  
 349 substantial eastern footprint also emerges from the East European Plain and Asia with 17%. The oceanic contributions from  
 350 the North Atlantic are 14% (compared to 24% in winter), and evaporation from the Black Sea provides 6% (similarly as in  
 351 winter). In the east, the Caspian Sea becomes a relevant moisture source with 3%. Some remote sources are also identified  
 352 over western Europe, Italy and the Balkans, but they are much weaker than those over eastern Europe and Ukraine.  
 353 In summer, contributions from remote moisture sources to EPEs in Ukraine are strongly reduced and evapotranspiration  
 354 from land is clearly the dominant source with 76% (Fig. 6b). Main local contributions are from eastern Europe (26%),

355 Ukraine (19%), and the Eastern European Plain (11%). The 24% of oceanic moisture sources of summer EPEs were  
 356 diagnosed from the Black Sea (8%), the midlatitude North Atlantic (7%), Western and Eastern Mediterranean (4%).  
 357 Moisture uptake from the Caspian Sea was weaker than in spring and autumn (2%). EPEs in autumn have also mainly  
 358 continental moisture sources (62%), mainly from eastern Europe (18%), Ukraine (13%), and Asia (12%). The influence  
 359 of oceanic moisture sources from western Mediterranean increases slightly compared to summer. The Black Sea becomes a  
 360 very important moisture source in this season with a 14% contribution. Also, considerable continental moisture recycling is  
 361 identified in the target region of the EPE, i.e. in the southern Ukraine. The maximum uptake is located around Crimea. And  
 362 finally, moisture uptake from the Caspian Sea was the largest compared to the other seasons (3%), most likely consistent  
 363 with advection from the east associated with the strongly negative MSLP anomalies in eastern Ukraine (Fig. 3d).  
 364



365  
 366  
 367 **Figure 7 Seasonal mean moisture sources for EPEs in Ukraine (%/10<sup>5</sup> km<sup>2</sup>).**

368  
 369 It is noteworthy, that there is less coherent structure in the fields of moisture sources compared to the upper-level circulation  
 370 fields investigated in the previous sections. This may be due to the fact that the upper-level circulation is often governed by  
 371 large-scale flow features, for example, the presence of a strong jet stream or a well-defined upper-level trough. This can  
 372 explain their somewhat more consistent structure compared to the more variable moisture sources. Since by far most of the  
 373 global water vapor is located in the lower troposphere, moisture source fields are influenced by factors like sea surface  
 374 temperatures, local evaporation, soil moisture availability, moisture transport, and low-level winds, and convection.  
 375 Winschall et al., (2014) investigated the importance of intensified local and remote evaporation for Mediterranean  
 376 precipitation extremes. Krug et al. (2022) determined that the evaporation anomalies are related to wind-speed anomalies  
 377 indicating mainly dynamically driven evaporation. Grams et al. (2014) emphasized the significant role of soil moisture

378 preconditioning. For instance, intense precipitation events can moisten the previously dry soil and might subsequently serve  
 379 as moisture sources for subsequent extreme EPEs (Bohlinger et al., 2017). And lastly, Dahinden et al. (2023) studied shallow  
 380 and deep convective systems that occur in random patches and lead to highly variable structure to the moisture source maps.  
 381 This complex interaction between various preconditioning factors and the eventually emerging moisture source patterns  
 382 should be investigated in more detail in future research.

383 In summary, this overview on seasonal moisture sources that contribute to EPEs in Ukraine reveals a large variability of the  
 384 sources, including local recycling and long-range transport over several 1000 km for instance from the central North Atlantic  
 385 (in winter and spring) and from the Caspian Sea (from spring to autumn). Oceanic moisture sources dominate in winter and  
 386 land moisture sources in all other seasons. Given that most EPEs in Ukraine occur in summer (Sect. 3.1) it becomes clear  
 387 that local recycling over Ukraine and land evapotranspiration over the neighboring regions (eastern Europe and the East  
 388 European Plain) are very important for understanding EPEs in Ukraine. And, in summer, the contributions from the Black  
 389 Sea are greater than those from the Mediterranean. This conclusion reflects that moisture fields can display high variability  
 390 and are influenced by a range of dynamic and local factors.

391 The principal results of the analysis of seasonal EPE characteristics in Ukraine are summarized in Table 1 to enhance clarity  
 392 and facilitate comparison. This allows us to contrast the results across seasons.

393

394 **Table 1 Mean seasonal characteristics of EPEs in Ukraine: Anomalies (units), moisture sources (MS, %) and affected**  
 395 **regions. Table abbreviations: W-west, E-east, S-south, N-north.**  
 396

	Winter	Spring	Summer	Autumn
Z <sub>500</sub>	Upper-level trough over E Europe & Ukraine: -241 m	Upper-level low over E & S Europe, Ukraine: -48 m	Upper-level low over the Balkans, the Black Sea & Ukraine: -43 m	Upper-level low over the Black Sea & Ukraine: -79 m
MSLP	Low over the Balkans: -24 hPa SE Ukraine: -20 hPa	Low over W & SW Ukraine: -6 hPa	Low over Ukraine: -4 hPa	Low over the Black Sea & E Ukraine: -12 hPa
PV (+)	Isentropic levels			
	315 K	325 K	335 K	330 K
	PV(+) north of 40°N: 0.1-2.5 PVU Cutoff over NE Black Sea region: 0.2-0.5 PVU	PV(+) over E Europe & W Ukraine: 1-2 PVU	Cutoff over the Balkans, Black Sea & SW Ukraine: 0.2-1 PVU	PV(+) over the Baltic region, N, Central & SW of Ukraine: 0.2-1 PVU; Cutoff over E Ukraine: 0.2-1 PVU
U <sub>300</sub>	SW jet stream over Mediterranean: +35 m·s <sup>-1</sup> , the Balkans: +30 m·s <sup>-1</sup> Ukraine, the Black & Azov Seas: +15-25 m·s <sup>-1</sup>	N jet stream over E Europe, the Balkans & W Ukraine: +10 m·s <sup>-1</sup>	Negative anomaly over W Ukraine: -10 m·s <sup>-1</sup> Positive anomaly over the Balkans & the Black Sea: +5 m·s <sup>-1</sup>	SW jet stream over the Black Sea & E Ukraine: +10 m·s <sup>-1</sup>
MS	1. North Atlantic (24 %), 2. Western Med (18 %) 3. Eastern Med (12 %) 4. Black Sea (7 %)	1. Eastern Europe (22 %) 2. North Atlantic (14 %) 3. Ukraine (14 %) 4. East European Plain & Asia (17 %) 5. Caspian Sea (3%)	1. Eastern Europe (25 %) 2. Ukraine (19 %) 3. East European Plain (11 %) 4. Black Sea (8 %) 5. North Atlantic (7 %) 6. Caspian Sea (2 %)	1. Eastern Europe (18 %) 2. Ukraine (13 %) 3. Asia (12 %) 4. N Atlantic & W Med (14 %) 5. Black Sea (14 %) 6. Azov Sea (3 %) 7. Caspian Sea (4 %)
EPE regions	W Ukraine, Crimea	W Ukraine, Crimea	Entire territory of Ukraine	W, SW & SE Ukraine, Crimea

397

### 398 3.5 Case studies of selected EPEs

399

400 After the climatological overview on EPEs in Ukraine given in the previous subsections, it is important to also show  
401 representative case studies of EPEs to obtain a more detailed understanding of the dynamics and associated moisture sources  
402 leading to the occurrence of these meteorological hazards. To this end, we selected eight events, two in each season. They  
403 are: (i) 28 December 1999 on the Crimean Peninsula; (ii) 21 December 1993 in western Ukraine; (iii) 15 May 2014 in the  
404 Transcarpathian region; (iv) 31 May 2014 in eastern Ukraine; (v) 1 July 2011 in central Ukraine; (vi) 1 August 2019 in  
405 southeastern Ukraine; (vii) 24 September 2014 in the Crimea; and (viii) 12 October 2016 in the northwestern Black Sea  
406 region. For each case, we briefly discuss the patterns of MSLP and surface precipitation, geopotential height at 500 hPa, and  
407 the identified moisture sources. Table S2 in the Supplement lists the relative contributions of the different moisture sources  
408 (Fig. 6a) for these cases.

409

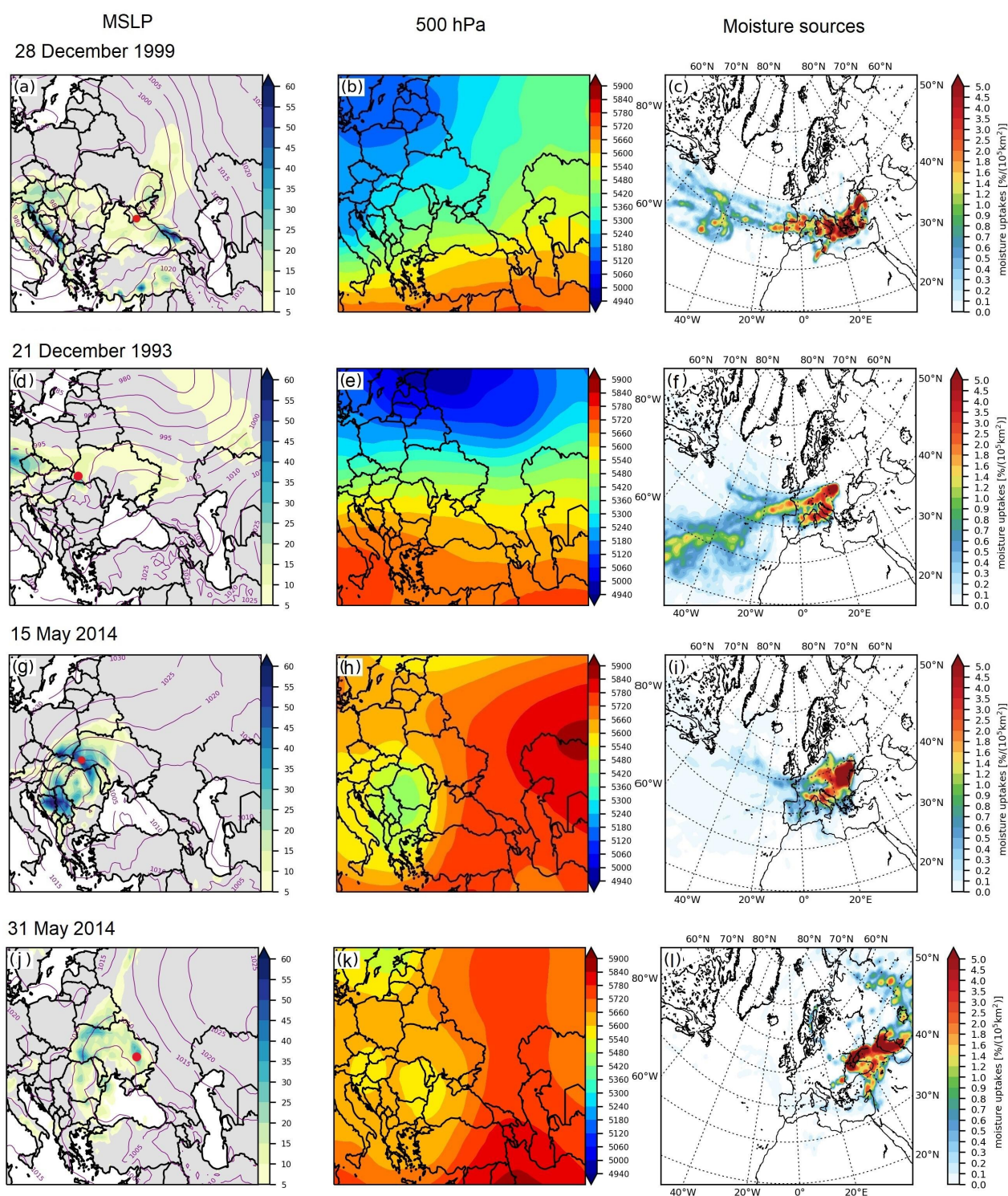
#### 410 3.5.1 Winter cases: 28 December 1999 and 21 December 1993

411

412 Both winter cases occurred under strong westerly flow and show common features and some distinctively different  
413 characteristics. The first EPE, on 27 and 28 December 1999, occurred two days after the infamous winter storm ‘Lothar’  
414 (24–26 December 1999) strongly damaged parts of France, Germany, and Switzerland. This storm developed beneath an  
415 exceptionally intense and zonally elongated westerly jet over the North Atlantic with wind speeds up to  $120 \text{ m}\cdot\text{s}^{-1}$   
416 (Wernli et al., 2002). In the next days, a series of cyclones moved from southeastern Europe over the northern coast of the  
417 Black and Azov Seas. One of the cyclones of this series caused extreme precipitation in the Crimean Peninsula.  
418 On 27 December,  $112.5 \text{ mm}\cdot\text{day}^{-1}$  were observed at Ai-Petri, and on 28 December  $100 \text{ mm}\cdot\text{day}^{-1}$  at Yalta with minor wave  
419 disturbances and  $115.3 \text{ mm}\cdot\text{day}^{-1}$  at Ai-Petri. The cyclone formed on 27 December in a short-wave perturbation over the  
420 Lower Danube Plain and the Black Sea Lowland between a deep Scandinavian low-pressure system and a high-pressure  
421 zone to the south. During 24 h it intensified rapidly and attained its minimum pressure of 990 hPa over Crimea and the Azov  
422 Sea. The largest precipitation values were registered close to the center of the cyclone (Fig. 8a). At upper levels there was an  
423 intense zonal flow with minor wave disturbances (Fig. 8b), which can be regarded as the extension of exceptional North  
424 Atlantic jet that led to the development of ‘Lothar’. It is remarkable, that one of the rare and most intense winter EPEs in  
425 Ukraine occurred right after one of the most severe winter storms in western and central Europe. The moisture sources for  
426 this EPE were mainly around Greece but extend in a zonal band far upstream into the central North Atlantic (Fig. 8c), i.e., in  
427 the region of rapid propagation of ‘Lothar’. Notable contributions were from the North Atlantic midlatitude (16-28 %),  
428 Western Mediterranean (19-24 %), Eastern Mediterranean (11-14 %) and the Black Sea (7-14 %).

429 The second winter EPE was on 21 December 1993 (Fig. 8d). During this event precipitation concentrated over the  
430 Transcarpathian region. The station Rahiv recorded  $101.4 \text{ mm}\cdot\text{day}^{-1}$ . The EPE was influenced by a surface cyclone that  
431 formed over southern Poland. As for the first case, an intense baroclinic zone with a strong upper-level zonal flow extended  
432 from the eastern North Atlantic in this case to the Caspian Sea. This went along with a deep low-pressure system over  
433 Scandinavia, the Baltic regions, the Kara Sea, and a high-pressure system over southern Europe and the Mediterranean  
434 (Fig. 8 d,e). The moisture sources were again extended far into the North Atlantic, in this case also with a substantial  
435 contribution from the subtropics. Other moisture sources were over continental areas of Europe and Ukraine (Fig. 8f). The  
436 largest contributions were from the North Atlantic mid- and subtropical latitudes (39% and 18%, respectively), and Western  
437 Mediterranean (14%). The terrestrial moisture sources, specifically Eastern Europe and Western Europe, made relatively  
438 minor contributions, accounting for 13% and 9%, respectively. Overall, long-range advection of oceanic moisture

439 contributed a major part to the winter EPEs. The percentage of oceanic moisture contributions was 54% on 28 December 1999  
 440 1999 and 68% on 21 December 1993.  
 441



442  
 443  
 444 **Figure 8** Overview on four EPE case studies (see dates on top of left panels), based on ERA-5. (a,d,g,j) show MSLP at  
 445 2100 UTC (purple contours, every 5 hPa) and daily accumulated total precipitation (mm, color shading), the  
 446 red dot indicates a station with precipitation > 100 mm·day<sup>-1</sup>; (b,e,h,k) show 500-hPa geopotential height at  
 447 2100 UTC (color shading, in m); and (c,f,i,l) show moisture uptake regions (in %/(10<sup>5</sup>km<sup>2</sup>).

### 448 3.5.2 Spring cases: 15 May 2014 and 31 May 2014

449

450 Both considered spring EPEs occurred in May 2014. They are interesting in that they affected different parts of Ukraine and  
451 had different moisture sources, despite a quite similar mid-tropospheric configuration. Between 14-16 May 2014, an EPE  
452 occurred in the Carpathians and Transcarpathia, with recorded values ranging from 106-145 mm·day<sup>-1</sup>, which corresponds to  
453 more than the monthly average. Concurrently, strong wind gusts exceeding 19 m·s<sup>-1</sup> were observed. These weather  
454 conditions led to severe flooding in the Dniester River basin. Additionally, the heavy rainfall triggered mudslides, affecting a  
455 total of 94 settlements, as documented by the European Severe Weather Database (ESWD, Dotzek, 2009). On 15 May,  
456 extended precipitation was observed in the Transcarpathian region, and 104.7 mm·day<sup>-1</sup> were recorded at Yaremche. The  
457 precipitation was caused by a deep cyclone (with a MSLP minimum of 1000 hPa) that formed over the Balkans on 14 May  
458 and reached Western Ukraine on 15 May (Fig. 8g). During the mature stage, an upper-level trough with a deep core formed  
459 over southeastern Europe and on 15 May overlapped with the surface cyclone (Fig. 8h). A large upper-level anticyclone in  
460 the east shaped a high-pressure belt over most parts of Ukraine and had a blocking effect, inhibiting further shifting of the  
461 cyclone to the northeast, which caused widespread precipitation over western Ukraine. Figure 8i shows that moisture sources  
462 for this EPE were mainly over Eastern Europe, Ukraine, Western Europe, and the Balkans with contributions of 37%, 19%,  
463 8%, and 8%, respectively. The North Atlantic plume of moisture contributed with 11%.

464 The second spring EPE occurred two weeks later, but in the east of Ukraine. On 31 May, 104.4 mm·day<sup>-1</sup> were recorded at  
465 Lozova. Damage was reported due to flooding, also to crops (ESWD, Dotzek, 2009). Precipitation was observed in a wide  
466 frontal band that formed between a cyclone that developed over Ukraine and the Black Sea with simultaneous intense  
467 anticyclogenesis over the East European Plain (Fig. 8j). At upper levels, a stationary trough extended from the north over  
468 East Europe and Ukraine with two centers of low pressure with similar intensity over Austria and Hungary, and over  
469 Bulgaria and Moldova (Fig. 8k). A strong ridge extended northward from Minor Asia and the Caspian Sea and again had a  
470 blocking-like signature affecting east Ukraine (Fig. 8k). In strong contrast to the previous three EPEs, moisture sources for  
471 this case were interestingly mainly further east. They stretched from the West Siberian Plain to the east Ukraine, the Black  
472 Sea, and east Turkey. The largest contributions were from Asia (28%) and Ukraine (15%). The moisture uptakes over the  
473 Caspian Sea, the Black Sea and the Azov Sea accounted for 15%, 13% and 6%, respectively (Fig. 8l).

474

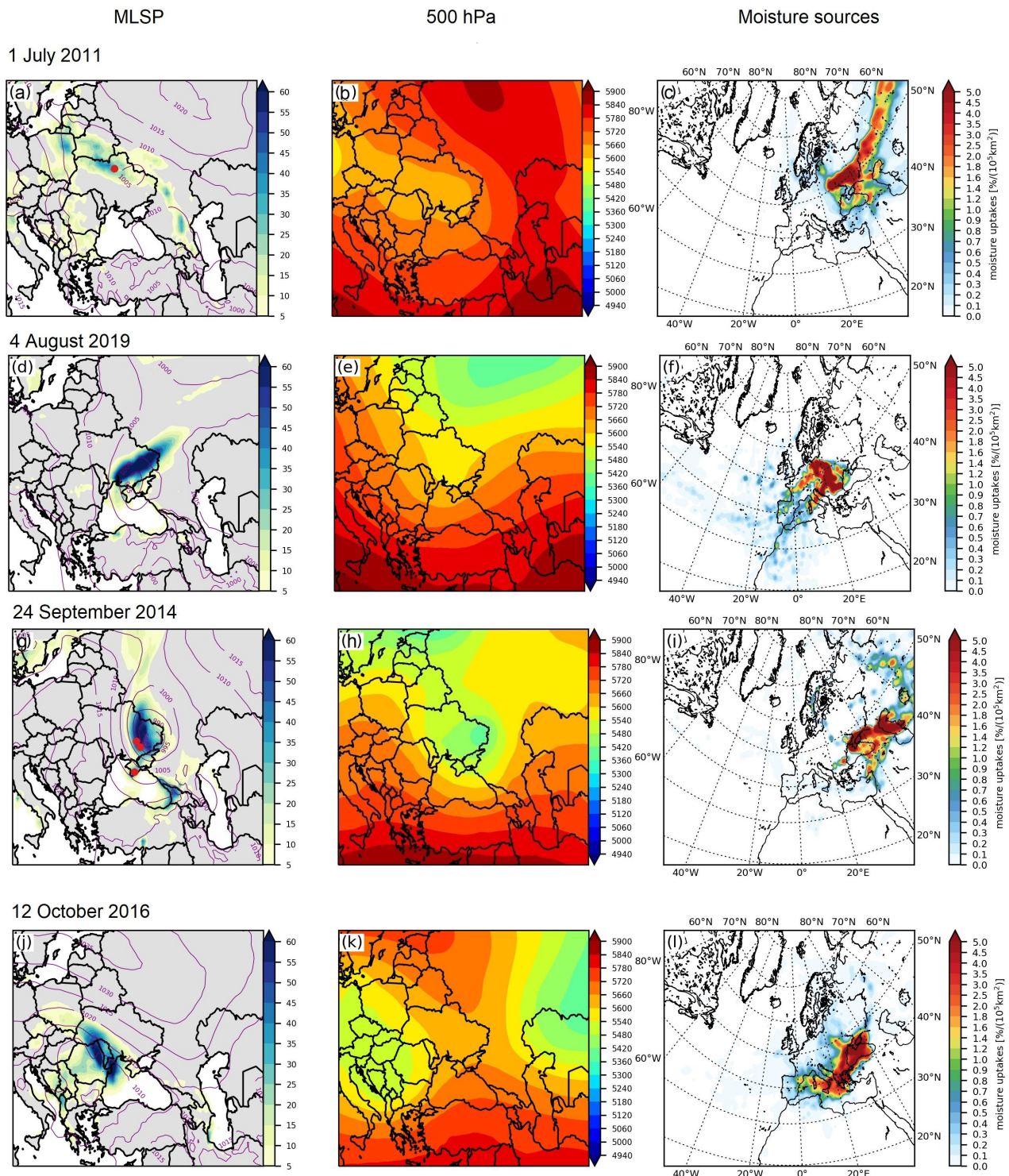
### 475 3.5.3 Summer cases: 1 July 2011 and 4 August 2019

476

477 The first selected EPE occurred on 1 July 2011, with precipitation spreading across the north of Ukraine. At Barishevka  
478 (Kyiv region) 130.5 mm·day<sup>-1</sup> were observed. Damage occurred due to flooding of local areas (ESWD, Dotzek, 2009). Two  
479 weak surface cyclones developed below an upper-level trough extending from Northern Europe, one over northeastern  
480 Ukraine and the other one east of the Black Sea, with central MSLP values of 1005 and 1010 hPa, respectively (Fig. 9a). An  
481 EPE formed in the northern regions of Ukraine along a cold front. Again, a blocking effect was exerted by a large  
482 anticyclone over the East European Plain. At upper levels, a stationary ridge associated with that surface high-pressure  
483 system spanned from the Middle East and Central Asia toward the north (Fig. 9b). Long-range transport of moisture is  
484 evident from three bands of moisture sources (Fig. 9c) A substantial amount of terrestrial moisture originated over Asia (32%)  
485 and the East European Plain (29%). Two other, much weaker, branches were formed over the Caspian Sea (2%) and the  
486 Black Sea basin (4%). Moisture uptake over Ukraine contributed with 19%.

487 The second summer EPE on 3-4 August 2019 was associated with heavy precipitation propagating across the southwest to  
488 the northeast of Ukraine along strong frontal systems associated with a cyclone moving from the Balkans towards eastern





489  
490  
491  
492  
493

**Figure 9** The same as Fig. 8 but for two EPEs each in summer and autumn (dates are indicated again on top of the left panels).

494 Ukraine (Fig. 9d). Combined with strong winds ( $15\text{--}24 \text{ m s}^{-1}$ ), this caused urban flooding and damaged energy infrastructure  
495 in the regions of Odesa, Kherson, Zaporozhye, Donetsk, Dnepropetrovsk and Lugansk (ESWD, Dotzek, 2009). Extreme  
496 precipitation was recorded at Belgorod Dnestrovsky in the Odesa region and at Khorli in the Kherson region with  $125.2$   
497  $\text{mm}\cdot\text{day}^{-1}$  and  $106.4 \text{ mm}\cdot\text{day}^{-1}$ , respectively. In this case, a pronounced upper-level trough extended from northern Russia

498 through Ukraine towards the Black Sea (Fig. 9e). A wide baroclinic zone occurred along the southern edge of the trough,  
499 stretching from southeastern Europe over the Black Sea to Middle Asia. This caused the formation of a strong northwesterly  
500 flow that advected relatively cool air to the Balkans, Turkey, and the western Black Sea. At the same time, warm air of  
501 tropical origin from Minor Asia and Caucasus propagated across the southeast of Ukraine and Crimea. On 3 August, the  
502 surface cyclone formed in a short-wave perturbation over the Balkans. The cyclone rapidly intensified and moved eastwards,  
503 made landfall in western Crimea 24 h later, where it reached its minimum MSLP below 995 hPa, and further passed on the  
504 eastern Ukraine. This EPE was characterized by a predominance of land evapotranspiration, accounting for 83% of the  
505 moisture. Notably, strong moisture contributions were observed in a large area of East Europe (48%) with additional  
506 moisture from West Europe, the Balkans and recycling over Ukraine. In contrast, oceanic contributions were relatively minor,  
507 with 9% from the North Atlantic midlatitude and 6% from the western Mediterranean (Fig. 9f).

#### 508 509 **3.5.4 Autumn cases: 24 September 2014 and 12 October 2016**

510  
511 On 23-24 September 2014, precipitation was observed mainly over southeastern and eastern Ukraine (Fig. 9g). Extreme  
512 precipitation was recorded at three stations: Prishib (Zaporizhzhia region, 114.7 mm·day<sup>-1</sup>), Sinelnikove (Dnipropetrovsk  
513 region, 100.1 mm·day<sup>-1</sup>), and Ai-Petri (Crimea, 107.8 mm·day<sup>-1</sup>). Major damage was caused by the strong winds (25 m s<sup>-1</sup>)  
514 and heavy precipitation (ESWD, Dotzek, 2009). A trough from north Russia towards the Black Sea developed on 22  
515 September and a deep closed cyclone over Crimea and the Azov Sea formed there on 23 September (Fig. 9h). This cutoff  
516 low system then propagated over Ukraine and the associated surface cyclone intensified strongly with central MSLP  
517 decreasing to 985 hPa (Fig. 9g) – the most intense cyclone in the considered case studies. Two stationary anticyclones,  
518 located over central Europe and over Russia, most likely exerted a blocking effect. The EPE resulted from a complex set of  
519 moisture sources (Fig. 9i). The main moisture sources were found over Asia (27%), the Eastern European Plain (18%), the  
520 Caspian Sea (18%), Ukraine (15%), and the Black Sea (13%).

521 The second autumn EPE occurred on 12-13 October 2016 with strong winds exceeding 25-31 m s<sup>-1</sup> and heavy precipitation  
522 over the Odesa region with 103 mm·day<sup>-1</sup> at Bolgrad on 12 October. Damage and four fatalities were reported due to winds  
523 and urban flooding (ESWD, Dotzek, 2009) and a state of emergency was declared in Odesa on 12 October. During this  
524 period, a quasi-stationary intense anticyclone was located over Scandinavia extending toward the Caspian Sea through most  
525 of the European part of Russia (Fig. 9j). At the same time, a cyclone developed over southern Europe, intensified to a MSLP  
526 minimum of 1005 hPa, and moved towards the northwest of the Black Sea. The precipitation area associated with a strong  
527 frontal system was extended along southwestern Ukraine and Moldova (Fig. 9j). On 12 October, a narrow upper-level ridge  
528 elongated over most of Ukraine, flanked by two upper-level cyclones (Fig. 9k). An intense baroclinic zone formed over  
529 southwestern Ukraine, within which the cyclone resided over the Odesa region for two days (not shown). This EPE shows a  
530 continuous band of moisture sources from the western Mediterranean to the Black Sea and south Ukraine (Fig. 9l). This  
531 event had a relatively large Black Sea moisture contribution (22%). The Black Sea is still quite warm in autumn, increasing  
532 the potential for intense evaporation. Other moisture sources for this event were mainly the Western (16%) and Eastern  
533 Mediterranean (9%), and the Balkans (12%).

534 Thus, this analysis of the large-scale flow conditions and moisture sources for eight different EPEs reveals a large variability  
535 from case to case. However, it is important to highlight that all EPEs, except those in winter, were influenced by a  
536 pronounced upper-level trough over Ukraine and a high-pressure system east or north of Ukraine. The most intense  
537 precipitation occurred during the EPE on 24 September 2014, when a cutoff formed and remained stationary over the target  
538 area. In stark contrast, the winter EPEs occurred in situations with exceptionally strong westerly jets. The local trough

539 configuration predominantly facilitated moisture sources of terrestrial origin and led to precipitation recycling over Ukraine  
540 during the EPEs days, whereas the winter EPEs had important long-range transport from the (subtropical) North Atlantic.

541

#### 542 **4 Summary and conclusions**

543

544 This study presents results of a climatological investigation of EPEs in Ukraine in the period 1979-2019. EPEs were  
545 identified with precipitation exceeding a simple threshold of  $100 \text{ mm}\cdot\text{day}^{-1}$  at measurement stations, and ERA5 reanalyses  
546 were used to investigate the large-scale physical and dynamical processes that were involved in the formation of these EPEs.  
547 In the following, provides a summary of the main results and the basis for addressing the four main aspects of EPEs  
548 investigated in this study, which are (1) the seasonal occurrence, frequency, and spatial distribution of EPEs in Ukraine, (2)  
549 the dynamical characteristics during EPEs, (3) the origin and transport pathways of moisture that led to the EPEs, and (4) the  
550 variability between individual cases.

551 1. Results show that Ukraine has two hotspots of EPE frequency: the Ukrainian Carpathians and Crimea. EPEs were  
552 recorded in all seasons in those regions. Nevertheless, in summer, during the season of maximum frequency of EPEs,  
553 they were observed not only in mountainous regions, but also across most other parts of Ukraine. In autumn, EPEs  
554 prevailed on the northwestern and northeastern coasts of the Black Sea.

555 2. EPEs occur due to relatively rare and anomalous circulation processes. Analysis of a combination of SLP and Z500  
556 anomalies, upper-level PV and 300-hPa winds has shown that: (i) negative anomalies of SLP and Z500 were found in all  
557 seasons, and PV streamers and cutoffs on 315–330 K occur in the key areas of cyclogenesis over Ukraine; (ii) anomalies  
558 of SLP and Z500, PV and 300-hPa wind show a clear connection with the observed EPEs over most of the studied  
559 domain, and with anomalies in total column water and, only in summer, in CAPE; (iii) isentropic potential vorticity  
560 anomalies associated with EPEs in Ukraine show distinct dipole patterns which changes from one season to the other,  
561 rotated by 90 degrees: northward in winter, westward in spring southward in summer, and eastward in autumn; (iv)  
562 winter, spring and autumn anomalies were distinguished by higher intensities compared to summer, however, EPEs were  
563 most frequently registered in summer and over the entire Ukraine. This might imply that, during summertime, the  
564 occurrence of EPEs in Ukraine is modulated not only by the large-scale circulation, but also by localized convection,  
565 which can play a significant role in shaping EPEs during this period.

566 3. The moisture source regions for the EPEs in each season in Ukraine have been investigated with a trajectory-based  
567 Lagrangian moisture source diagnostic. The results show that EPEs mainly in winter were associated with long-range  
568 atmospheric moisture transport of oceanic origin, which occurred southward of the maximum positive PV anomaly  
569 region. Moisture uptake regions were the subtropical and midlatitude North Atlantic, and the Mediterranean. However,  
570 during the other seasons, terrestrial moisture sources dominated in contributing to EPEs. In spring and autumn, the  
571 moisture contributions from land surfaces represented mainly a combination of different local sources and additional  
572 remote sources, both from the European continent and from Asia. Evaporation from the North Atlantic in spring and  
573 from the Mediterranean Sea in autumn, in combination with transport from the Caspian Sea provided moisture from  
574 ocean sources during those seasons. A correlation with PV dipoles localization was also observed: the predominance of  
575 moisture flows from remote sources on the southeastern flank of the positive PV anomaly in spring and along the  
576 southwestern edge in autumn. In summer, the primary source of moisture over Ukraine was land evapotranspiration,  
577 mainly from Eastern Europe, Ukraine, and the East European Plain, and the area of maximum moisture uptake  
578 practically overlapped with the region of positive PV. It is worth noting the contribution of the Black Sea as a local

579 source of moisture, which is an important oceanic source region that provided year-round moisture to EPEs along the  
580 south coast, as well as some continental regions of Ukraine.

581 4. Analysis of large-scale flow conditions and moisture source regions for individual events, based on ERA5 data, has  
582 confirmed that EPE generation in spring, summer, and autumn was mainly due to the impact of upper-level troughs  
583 extending over eastern and southern Europe and blocking anticyclone over the Eastern European Plain. In the western  
584 and southwestern regions of Ukraine, cutoffs formed during some EPEs. The exception were winter EPEs, when the  
585 cyclones formed due to a short-wave perturbation in the westerly flow, which delivered moist air from the North  
586 Atlantic and the Mediterranean to western and southern Ukraine. The study of the moisture sources for eight EPEs in  
587 Ukraine showed important case-to-case variability. This indicates, very importantly, that seasonal mean conditions are  
588 not necessarily representative for individual EPEs, and that even two EPEs occurring in the same month (see the two  
589 EPEs selected in May 2014) can have very different moisture sources despite relatively similar patterns in 500-hPa  
590 geopotential height. Clearly this field, often investigated in synoptic climatologies, cannot fully represent the complex  
591 dynamics and moisture transport at multiple scales involved in EPEs.

## 593 References

594  
595 Aemisegger, F., Pfahl, S., Sodemann, H., Lehner, I., Seneviratne, S.I., Wernli, H.: Deuterium excess as a proxy for  
596 continental moisture recycling and plant transpiration, *Atmos. Chem. Phys.*, 14(8):4029–4054, <https://doi.org/10.5194/acp-14-4029-2014>, 2014.

598 Aemisegger, F.: On the link between the North Atlantic storm track and precipitation deuterium excess in Reykjavik, *Atmos.*  
599 *Sci. Lett.*, 19, e865, <https://doi.org/10.1002/asl.865>, 2018.

600 Agel, L., and Barlow, M., Colby, F., Binder, H., Catto, J. L., Hoell, A. and Cohen, J.: Dynamical analysis of extreme  
601 precipitation in the US northeast based on large-scale meteorological patterns, *Clim. Dyn.*, 50, 1819–1839,  
602 <https://doi.org/10.1007/s00382-018-4223-2>, 2018.

603 Armon, M., de Vries, A. J., Marra, F., Peleg, N., and Wernli, H.: Saharan rainfall climatology and its relationship with  
604 surface cyclones, *Weather Clim. Extremes*, 43, 100638, <https://doi.org/10.1016/j.wace.2023.100638>, 2024.

605 Barton, Y., Giannakaki, P., von Waldow, H., Chevalier, C., Pfahl, S. and Martius, O.: Clustering of regional-scale extreme  
606 precipitation events in southern Switzerland, *Mon. Wea. Rev.*, 144, 347–369, <https://doi.org/10.1175/MWR-D-15-0205.1>,  
607 2016.

608 Bohlinger, P., Sorteberg, A., and Sodemann, H.: Synoptic conditions and moisture sources actuating extreme precipitation  
609 in Nepal. *J. Geophys. Res.: Atmos.*, 122, 12,653–12,671, <https://doi.org/10.1002/2017JD027543>, 2017.

610 Boissier, L., and Vinet, F.: Paramètres hydroclimatiques et mortalité due aux crues torrentielles: Etude dans le sud de la  
611 France. XXIIème colloque de l'Association Internationale de Climatologie, 1-5 Sept. 2009, Cluj-Napoca, Roumanie.  
612 pp.79-84, (hal-03069229), 2009.

613 Breugem A. J., Wesseling, J. G., Oostindie, K., and Ritsema, C. J.: Meteorological aspects of heavy precipitation in relation  
614 to floods – An overview, *Earth-Science Reviews*, V.204, 103171, ISSN 0012-8252,  
615 <https://doi.org/10.1016/j.earscirev.2020.103171>, 2020.

616 Budyko, M. I., and Drozdov O. A.: Zakonomernosti vlogooborota v tmosphere (regularities of the hydrologic cycle in the  
617 atmosphere), *Izv. Akad. Nauk SSSR Ser. Geogr.*, 4, 5–14,

618 [http://scholar.google.com/scholar\\_lookup?title=Climate+and+Life.&author=M.+I.+Budyko&publication\\_year=1974](http://scholar.google.com/scholar_lookup?title=Climate+and+Life.&author=M.+I.+Budyko&publication_year=1974), 1953.

619 Catto, J. L., and Pfahl, S.: The importance of fronts for extreme precipitation, *J. Geophys. Res.*, 118, 10, 791–10, 801,  
620 <https://doi.org/10.1002/jgrd.50852>, 2013.

621 Ciric, D., Nieto, R., Losada, L., Drumond, and A., Gimeno, L.: The Mediterranean moisture contribution to climatological  
622 and extreme monthly continental precipitation, *Water* 10(4):519, <http://www.mdpi.com/2073-4441/10/4/519>, 2018.

623 Dahinden, F., Aemisegger, F., Wernli, H., and Pfahl, S.: Unravelling the transport of moisture into the Saharan Air Layer  
624 using passive tracers and isotopes, *Atmospheric Science Letters*, 24, e1187, <https://doi.org/10.1002/asl2.1187>, 2023.

625 de Vries, A. J.: A global climatological perspective on the importance of Rossby wave breaking and intense moisture  
626 transport for extreme precipitation events, *Weather Clim. Dynam.*, 2, 129–161, <https://doi.org/10.5194/wcd-2-129-2021>,  
627 2021.

628 Dotzek, N., P. Groenemeijer, B. Feuerstein, and A. M. Holzer: Overview of ESSL's severe convective storms research using  
629 the European Severe Weather Data-base ESWD, *Atmos. Res.*, 93, 575–86, <https://doi.org/10.1016/j.atmosres.2008.10.020>,  
630 2009.

631 Gao, X., and Mathur, S.: Predictability of U.S. regional extreme precipitation occurrence based on large-scale meteorological  
632 patterns (LSMPs), *J. Climate*, 34, 7181–7198, <https://doi.org/10.1175/JCLI-D-21-0137.1>, 2021.

633 Giuntoli, I., Fabiano, F. and Corti, S.: Seasonal predictability of Mediterranean weather regimes in the Copernicus C3S  
634 systems, *Clim. Dyn.*, 58, 2131–2147, <https://doi.org/10.1007/s00382-021-05681-4>, 2022.

635 Grams, C. M., Binder, H., Pfahl, S., Piaget, N., and Wernli, H.: Atmospheric processes triggering the central European  
636 floods in June 2013, *Nat. Hazards Earth Syst. Sci.*, 14, 1691–1702, <https://doi.org/10.5194/nhess-14-1691-2014>, 2014.

637 Gimeno, L., A. Stohl, R. M., Trigo, F., Dominguez, K., Yoshimura, L.-Yu, Drumond, A., Durán-Quesada, A. M., and Nieto,  
638 R.: Oceanic and terrestrial sources of continental precipitation, *Rev. Geophys.*, 50, RG4003,  
639 <https://doi.org/10.1029/2012RG000389>, 2012.

640 Hersbach, H., and Coauthors: The ERA5 global reanalysis, *Quart. J. Roy. Meteor. Soc.*, 146, 1999–2049,  
641 <https://doi.org/10.1002/qj.3803>, 2020.

642 Horan, M.F., Batibeniz, F., Kucharski, F., Almazroui, M., Abid, M.A., Fu, J.S., and Ashfaq, M.: Moisture sources for  
643 precipitation variability over the Arabian Peninsula, *Clim. Dyn.*, 61, 4793–4807, [https://doi.org/10.1007/s00382-023-06762-](https://doi.org/10.1007/s00382-023-06762-2)  
644 2, 2023.

645 In Masson-Delmotte, V., Zhai, P., Pirani, A., Connors, S. L., Péan, C., Berger, S. et al. (Eds.): Summary for policymakers.  
646 Climate change 2021: The physical science basis. Contribution of working group I to the sixth assessment report of the  
647 intergovernmental panel on climate change, IPCC, Cambridge University Press, <https://www.ipcc.ch/report/ar6/wg1/>, 2021.

648 Jonkman, S.N.: Global perspectives on loss of human life caused by floods, *Nat. Hazards*, 34, 151–175,  
649 <https://doi.org/10.1007/s11069-004-8891-3>, 2005.

650 James, P. and Stohl A.: A Lagrangian analysis of the atmospheric branch of the global water cycle. Part I: Method description,  
651 validation, and demonstration for the August 2002 flooding in Central Europe, *J. Hydrometeor.*, 5, 656–678,  
652 [https://doi.org/10.1175/1525-7541\(2004\)005%3C0656:ALAOTA%3E2.0.CO;2](https://doi.org/10.1175/1525-7541(2004)005%3C0656:ALAOTA%3E2.0.CO;2), 2004.

653 Jonkeren, O., Rietveld, P., van Ommeren, J., and Linde, A.: Climate change and economic consequences for inland  
654 waterway transport in Europe, *Reg. Environ. Change*, 14, 953–965, <https://doi.org/10.1007/s10113-013-0441-7>, 2014.

655 Kautz, L.-A., Martius, O., Pfahl, S., Pinto, J., Ramos, A., Sousa, P., and Woollings, T.: Atmospheric blocking and weather  
656 extremes over the Euro-Atlantic sector – A review, *Weather Clim. Dynam.*, 3, 305–336, <https://doi.org/10.5194/wcd-2021-56>,  
657 2022.

658 Krug, A., Aemisegger, F., Sprenger, M., and Ahrens, B.: Moisture sources of heavy precipitation in Central Europe in  
659 synoptic situations with Vb-cyclones, *Clim. Dyn.*, 59, 3227–3245, <https://doi.org/10.1007/s00382-022-06256-7>, 2022.

660 Läderach, A., and Sodemann, H.: A revised picture of the atmospheric moisture residence time, *Geophys. Res. Lett.*, 43,  
661 924–933, <https://doi.org/10.1002/2015GL067449>, 2016.

662 Lenggenhager, S., and Martius, O.: Atmospheric blocks modulate the odds of heavy precipitation events in Europe, *Clim.*  
663 *Dyn.*, 53, 4155–4171, <https://doi.org/10.1007/s00382-019-04779-0>, 2019.

664 Li, J., and Wang, B.: Predictability of summer extreme precipitation days over eastern China, *Clim. Dyn.*, 51, 4543–4554,  
665 <https://doi.org/10.1007/s00382-017-3848-x>, 2018.

666 Lipinskiy, V.M., Diachuk, V.A. and Babichenko, V.M. (eds): *Klimat Ukrainy [Climate of Ukraine]*, Kyiv: Raevsky Publ.,  
667 Ukraine, 2003.

668 Lipinskiy, V.M., Osadchy, V., Shestopalov, V.M., Rudenko, L.G., Dmytrenko, V.P., Martazinova, V.F., Nabivanets, Y.B.,  
669 Babichenko, V.N., Kulbida, N.Y., and Shereshevsky, A.I.: *Atlas "Climate and water resources of Ukraine"*, K.: Nika Center,  
670 [https://uhmi.org.ua/conf/climate\\_changes/presentation\\_pdf/plenary\\_session/Lipinskiy\\_et\\_al.pdf](https://uhmi.org.ua/conf/climate_changes/presentation_pdf/plenary_session/Lipinskiy_et_al.pdf), 2011.

671 Liniger, M. A., and Davies, H. C.: Seasonal differences in extratropical potential vorticity variability at tropopause levels,  
672 *J. Geophys. Res.*, 109, <https://doi.org/10.1029/2004JD004639>, 2004.

673 Madsen, H., Lawrence, D., Lang, M., Martinkova, M., and Kjeldsen, T. R.: Review of trend analysis and climate change  
674 projections of extreme precipitation and floods in Europe, *J. Hydrol.*, 519, 3634– 3650, doi:10.1016/j.jhydrol.2014.11.003,  
675 2014.

676 Martin-Vide, J., Sanchez-Lorenzo, A., Lopez-Bustins, J. A., Cordobilla, M. J., Garcia-Manuel, A., and Raso, J. M.:  
677 Torrential rainfall in northeast of the Iberian Peninsula: synoptic patterns and WeMO influence, *Adv. Sci. Res.*, 2, 99–105,  
678 <https://doi.org/10.5194/asr-2-99-2008>, 2008.

679 Mastrantonas, N., Magnusson, L., Pappenberger, F., and Matschullat, J.: Extreme precipitation events in the Mediterranean:  
680 Spatiotemporal characteristics and connection to large-scale atmospheric flow patterns, *Quart. J. Roy. Meteor. Soc.*, 148,  
681 875-890, <https://doi.org/10.1002/joc.6985>, 2020.

682 Mastrantonas, N., Magnusson, L., Pappenberger, F., Matschullat, J.: What do large-scale patterns teach us about extreme  
683 precipitation over the Mediterranean at medium- and extended-range forecasts?, *Quart. J. Roy. Meteor. Soc.*, 148, 875-890,  
684 <https://doi.org/10.1002/qj.4236>, 2021.

685 Massacand, A.C., Wernli, H., and Davies, H.C.: Heavy precipitation on the Alpine southside: an upper-level precursor,  
686 *Geophys. Res. Lett.*, 25, 1435–1438, <https://doi.org/10.1029/98GL50869>, 1998.

687 Martazinova, V., and Shcheglov, A.: Nature of extreme precipitation over Ukraine in the 21st century, *Ukr. Hydromet. J.*, 22,  
688 36-45, <https://doi.org/10.31481/uhmj.22.2018.04>, 2018.

689 Mykhailiuk, R.: Measures to protect the principal Carpathia from disasterable floods by analysis of their causes and  
690 consequences in 2008 and 2020. *Ecological Safety and Balanced Use of Resources*, 2(24), 13–26,  
691 [https://doi.org/10.31471/2415-3184-2021-2\(24\)-13-26](https://doi.org/10.31471/2415-3184-2021-2(24)-13-26), 2022.

692 Moore, B. J., Keyser, D., and Bosart, L. F.: Linkages between extreme precipitation events in the central and eastern United  
693 States and Rossby wave breaking, *Mon. Wea. Rev.*, 147, 3327–3349, <https://doi.org/10.1175/MWR-D-19-0047.1>, 2019.

694 Moore, B. J., White, A. B., Gottas, D. J., and Neiman, P. J.: Extreme precipitation events in Northern California during  
695 winter 2016–17: Multiscale analysis and climatological perspective, *Mon. Wea. Rev.*, 148, 1049–1074,  
696 <https://doi.org/10.1175/MWR-D-19-0242.1>, 2020.

697 Osadchy, V., and Babichenko, V.: Dynamics of extreme meteorological phenomena in Ukraine, *Ukrainian Geograph. J.*, 4,  
698 8-14, <https://ukrgeojournal.org.ua/en/node/345>, 2012.

699 Papritz, L., Aemisegger, F., and Wernli, H.: Sources and Transport Pathways of Precipitating Waters in Cold-Season Deep  
700 North Atlantic Cyclones, *J. Atmos. Sci.*, 78, 3349-3368, <https://doi.org/10.1175/JAS-D-21-0105.s1>, 2021.

701 Pfahl, S.: Characterising the relationship between weather extremes in Europe and synoptic circulation features, *Nat.*  
702 *Hazards Earth Syst. Sci.*, 14, 1461–1475, <https://doi.org/10.5194/nhess-14-1461-2014>, 2014.

703 Pfahl, S. and Wernli, H.: Quantifying the relevance of cyclones for precipitation extremes, *J. Climate*, 25, 6770–6780,  
704 <https://doi.org/10.3929/ethz-b-000057303>, 2012.

705 Portmann, R., Sprenger, M., and Wernli, H.: The three-dimensional life cycles of potential vorticity cutoffs: a global and  
706 selected regional climatologies in ERA-Interim (1979–2018), *Weather Clim. Dynam.*, 2, 507–534,  
707 <https://doi.org/10.5194/wcd-2-507-2021>, 2021.

708 Priestley, M. D. K., Pinto, J. G., Dacre, H. F., and Shaffrey, L. C.: The role of cyclone clustering during the stormy winter of  
709 2013/2014, *Weather*, 72, 187–192, <https://doi.org/10.1002/wea.3025>, 2017.

710 Rasmussen, K. L., and R. A. Houze Jr.: Convective initiation near the Andes in subtropical South America. *Mon. Wea.*  
711 *Rev.* 144. 2351–2374. <https://doi.org/10.1175/MWR-D-15-0058.1>, 2016.

712 Raveh-Rubin, S., and Wernli, H.: Large-scale wind and precipitation extremes in the Mediterranean: dynamical aspects of  
713 five selected cyclone events, *Quart. J. Roy. Meteor. Soc.*, 142(701), 3097– 3114, <https://doi.org/10.1002/qj.2891>, 2016.

714 Rex, D.F.: Blocking action in the middle troposphere and its effect upon regional climate: I. An aerological study of blocking  
715 action. *Tellus*, 2, 196–211, <https://doi.org/10.3402/tellusa.v2i3.8546>, 1950.

716 Santos, J. A., Belo-Pereira, M., Fraga, H., and Pinto, J. G.: Understanding climate change projections for precipitation over  
717 western Europe with a weather typing approach, *J. Geophys. Res. Atmos.*, 121, 1170–1189,  
718 <https://doi.org/10.1002/2015JD024399>, 2016.

719 Semerhei-Chumachenko, A., and Slobodanyk, K.: Spatial–temporal distribution of heavy precipitation over Ukraine during  
720 1979-2019 according to the ERA5 reanalysis, *Ukr. Hydromet. J.*, 26, <https://doi.org/10.31481/uhmj.26.2020.04>, 2020.

721 Sprenger, M., and Wernli, H.: The LAGRANTO Lagrangian analysis tool – version 2.0, *J. Geosci. Model Dev.*, 8, 2569–  
722 2586, <https://doi.org/10.5194/gmd-8-2569-2015>, 2015.

723 Sodemann, H., Schwierz, C., and Wernli, H.: Interannual variability of Greenland winter precipitation sources: Lagrangian  
724 moisture diagnostic and North Atlantic Oscillation influence, *J. Geophys. Res.*, 113, <https://doi.org/10.1029/2007JD008503>,  
725 2008.

726 Sodemann, H.: Beyond Turnover Time: Constraining the Lifetime Distribution of Water Vapor from Simple and Complex  
727 Approaches, *J. Atmos. Sci.*, 77, 413–433, <https://doi.org/10.1175/JAS-D-18-0336.1>, 2020.

728 Sodemann, H. and Zubler, E.: Seasonal and inter-annual variability of the moisture sources for Alpine precipitation during  
729 1995-2002, *Int. J. Climatol.*, 30, 947–961, <https://doi.org/10.1002/joc.1932>, 2009.

730 Trambly, Y., Neppel, L., Carreau, J., and Najib, K.: Non-stationary frequency analysis of heavy rainfall events in southern  
731 France: *Hydrological Sciences Journal*, 58 (2), 280–294, <https://doi.org/10.1080/02626667.2012.754988>, 2013.

732 Tuel, A., Martius, O.: Subseasonal Temporal Clustering of Extreme Precipitation in the Northern Hemisphere:  
733 Regionalization and Physical Drivers, *J. Clim.*, 35 (11), 3537–3555, <https://doi.org/10.1175/JCLI-D-21-0562.1>, 2022.

734 Ukrainian State Agency of Water Resources: [https://davr.gov.ua/korotkij-oglyad-potochnoi-vodnoi-situacii-v-richkovih-](https://davr.gov.ua/korotkij-oglyad-potochnoi-vodnoi-situacii-v-richkovih-basejnah-ukraini-stanom-na-26062020)  
735 [basejnah-ukraini-stanom-na-26062020](https://davr.gov.ua/korotkij-oglyad-potochnoi-vodnoi-situacii-v-richkovih-basejnah-ukraini-stanom-na-26062020), last access: 27 March 2024, 2020.

736 Wernli, H., Dirren, S., Liniger, M. A., and Zillig, M.: Dynamical aspects of the life cycle of the winter storm ‘Lothar’ (24–26  
737 December 1999), *Quart. J. Roy. Meteor. Soc.*, 128, 405–429, <https://doi.org/10.1256/003590002321042036>, 2002.

738 Winschall, A., Sodemann, H., Pfahl S., and Wernli H.: How important is intensified evaporation for Mediterranean  
739 precipitation extremes?, *J. Geophys. Res. Atmos.*, 119, 5240–5256, <https://doi.org/10.1002/2013JD021175>, 2014.

740 Yang, Z., Qian, Y., Xue, P., Wang, J., Chakraborty, T. C., Pringle, W. J., Li, J., and Chen, X. : Moisture sources of  
741 precipitation in the Great Lakes Region: Climatology and recent changes. *Geophys. Res. Lett.*, 50, e2022GL100682,  
742 <https://doi.org/10.1029/2022GL100682>, 2023.

743

744 **Data availability**

745 ERA5 data is openly available at <https://cds.climate.copernicus.eu> (Hersbach et al., 2020). The observational data used for  
746 this study can be requested from the Central Geophysical Observatory in Ukraine (<http://cgo-sreznevskyi.kyiv.ua/en/>).

747 **Author contributions**

748 EA and HW designed and planned the study, EA performed the analysis, and wrote the manuscript with support from HW.  
749 Visualizations were produced by MA, FA, AS and EA. All authors contributed to the interpretation and discussion of the  
750 results.

751 **Competing interests**

752 The authors declare that they have no conflict of interest.

753 **Acknowledgements**

754 EA is grateful to OSENU (Odesa State Environmental University) for providing the precipitation observations from Ukraine.  
755 The authors also thank the reviewers for their constructive feedback that helped improving the presentation of the results.

756 **Financial support**

757 EA and AS were supported by the Swiss National Science Foundation (grant no. 212026 and 216775, and 188660,  
758 respectively). MA was supported by an ETH Zürich postdoctoral fellowship (project no. 21-1 FEL67) and by the Stiftung für  
759 naturwissenschaftliche und technische Forschung as well as the ETH Zürich Foundation.

760